Relationship between Bulk Phase, Near Surface and Outermost Atomic Layer of VPO Catalysts and their Catalytic Performance in the Oxidative Dehydrogenation of Ethane

Francisco Ivars-Barceló,[a,#1,*] Graham J. Hutchings,[b] Jonathan K. Bartley,[b] Stuart H. Taylor,[b] Peter Sutter,[a,#2] Pedro Amorós,[c] Rut Sanchis,[d] Benjamín Solsona.[d,*]

[a] Center for Functional Nanomaterials, Brookhaven National Laboratory, Upton, New York 11973 (USA). E-mail: accfib@hotmail.com

[b] Cardiff Catalysis Institute, School of Chemistry, Cardiff University, Main Building, Park Place, Cardiff, CF10 3AT (UK).

[c] Instituto de Ciencia de los Materiales (ICMUV), Universitat de València, Av. Universitat s/n,46100 Burjassot-Valencia (Spain)

[d] Department of Chemical Engineering, Universitat de València, Av. Universitat s/n,

46100 Burjassot-Valencia (Spain). E-mail: benjamin.solsona@uv.es

[#1] Present address: Fritz-Haber-Institut der Max-Planck-Gesellschaft, Faradayweg 4-6, 14195 Berlin (Germany). E-mail: fivars@fhi-berlin.mpg.de

[#2] Present address: Department of Electrical and Computer Engineering, University of Nebraska-Lincoln, Lincoln, Nebraska 68588 (USA)

Abstract

A set of vanadium phosphorous oxide (VPO) catalysts, mainly consisting of $(VO)_2P_2O_7$, $VO(PO_3)_2$ or $VOPO_4{\cdot}2H_2O$ bulk crystalline phases, has been investigated for the oxidative dehydrogenation (ODH) of ethane to ethylene, a key potential reaction for a sustainable industrial and socioeconomic development. The catalytic performance on these VPO catalysts has been explained on the basis of the main crystalline phases and the corresponding surface features found by XPS and LEISS at 400 ºC, *i.e.* within the temperature range used for ODH reaction. The catalysts based on $(VO)_2P_2O_7$ phase presented the highest catalytic activity and productivity to ethylene. Nevertheless, the catalysts consisting of $VO(PO_3)_2$ structure showed higher selectivity to ethylene, reaching 90% selectivity at *ca.* 10% ethane conversion. To the best of our knowledge, this is the highest selectivity reported on a vanadium phosphorous oxide at similar conversions for the ethane ODH. In general, catalysts consisting of crystalline phases with vanadium present as V^{4+}, i.e. $(VO)_2P_2O_7$ and $VO(PO_3)_2$, were found to be significantly more selective to ethylene than those containing V^{5+} phases. The surface analysis by XPS showed an inverse correlation between the mean oxidation state of vanadium near surface and the selectivity to ethylene. The lower averaged oxidation states of vanadium appear to be favoured by the presence of V^{3+} species near the surface, which was only found in the catalysts containing V^{4+} phases. Among those catalysts the one based on $VO(PO_3)_2$ phase shows the highest selectivity, which could be related to the most isolated scenario of V species (the lowest V content relative to P) found at the outermost surface by low energy ion scattering spectroscopy (LEISS), a "true" surface technique only sensitive to the outermost atomic layer.

Keywords: Ethane; ethylene; oxidative dehydrogenation; vanadium phosphorous oxide; vanadyl pyrophosphate; VPO; ion scattering; LEISS; XPS.

Introduction

Ethylene is considered a very important building block in the petrochemical industry. Additionally, in the foreseeable future an increase in both worldwide ethylene production and demand is expected, although with a highly uneven geographic distribution. China and other Asian countries currently dominate both supply and demand. An increase in ethylene production is predicted in the US due to the low cost of ethane supplies from shale gas, whereas Western European countries show a slowing ethylene production.

The current low cost of ethane in the US is providing the basis for an increased investment in large-scale steam cracker projects, whereas in China new research is being conducted to develop coal-based technologies to obtain ethylene. However, both the conventional steam cracking and the possible coal-based technologies are not considered to be environmentally friendly processes. Coal is the most polluting among the fossil resources, whereas steam-cracking is one of the highest energy consuming industrial processes, and has practical problems, such as a tendency toward coke formation, which results in low selectivity towards olefins [1,2,3].

In view of this situation, oxidative dehydrogenation (ODH) of ethane is becoming increasingly popular as an alternative to steam cracking, since it can prevent some of the issues associated with that inefficient process. ODH is an exothermic reaction and coke is not formed as the catalyst is regenerated in-situ by co-fed oxygen [4-7]. At present, the most promising catalytic systems for ODH of ethane are based on MoVTeNb oxides

[8-12] and promoted NiO [13-19]. Nevertheless, further research is needed in order to set the foundation for developing optimized industrial processes based on ODH technology.

Catalysts based on vanadium and phosphorus oxides (VPO) have also been studied for ODH of ethane, but to a lesser extent. V-P-O catalysts are the commercial catalysts for the selective oxidation of n-butane to maleic anhydride [20-22], the first heterogeneously catalyzed process based on alkane selective oxidation commercialized on a large-scale. Although the first work and patents date back to the 70's [23,24,25] there are still some uncertainties among researchers with respect to the performance of VPO catalysts for this process. Nevertheless there are also some general agreement [21,26,27,28]. Thus, it seems clear that $(VO)_2P_2O_7$ must be the main crystalline phase of the catalysts and the optimal catalyst must present an enrichment of phosphorus (P/V > 1 at. ratio). Moreover, the oxidation state of vanadium must be close to +4 (between 4 and 4.1), although the presence of V^{5+} species in low concentrations can also play an important role. The hydrogen abstraction (activation of n-butane) seems to be the rate determining step, taking place on V-species. One of the characteristics that differentiate VPO catalysts from other catalytic systems is their complex activation, as the surface shows highly dynamic behaviour. In fact the variations in conversion and selectivity to maleic anhydride can change remarkably by slightly modifying the feed composition, flow and/or the activation treatment [29,30,31]. Overall, this commercial process has evolved for the past 4 decades from the first patent published by researchers of Monsanto in 1974 [25] with yields to maleic anhydride not exceeding 30%, to current values higher than 65% claimed by researchers from Lonza [32].

Although industrial catalysts contain $(VO)_2P_2O_7$ as the main crystalline phase, some other V-P-O phases have also been shown to be capable of activating n-butane to yield maleic anhydride, e.g. the $VO(PO_3)_2$ phase [33].

Regarding the use of VPO catalysts in ODH of ethane, just a few relevant studies appear in the literature. Nevertheless, further research on VPO based catalysts is encouraged by the fact that they have already been established for an oxidative industrial process, the selective oxidation of n-butane to maleic anhydride Loukah *et al.* [34] showed that vanadyl pyrophosphate was reasonably selective to ethylene, but at low ethane conversions. The incorporation of some additives with large ionic radii have been reported to distort the structure of vanadyl pyrophosphate, increasing the catalytic activity [35,36]. The addition of dopants such as Zr^{4+} and Bi^{3+}, for example, have resulted in enhanced catalytic activity while maintaining the same selectivity to ethylene as found for the unpromoted VPO catalyst. This behaviour was explained by the enhanced surface area and to a lower O(1s) binding energy [37,38]. However, if La was added the selectivity and the catalytic activity dropped, due to the formation of $VOPO_4$, which showed a much poorer catalytic performance than the $(VO)_2P_2O_7$ phase. In other work, the addition of promoters to VPO led to a higher overall rate of the reaction, but the selectivity to ethylene had a complex trend [39].

Zazhigalov *et al.* [40] tested VPO catalysts supported on different oxides, such as TiO_2 and high surface areas silica by a mechano-chemical treatment, and no differences were observed in the ethane ODH compared to the classical bulk VPO catalysts. The advantage of a supported catalyst was claimed to be a lower consumption of organic acids during the preparation procedure. Similarly Lisi *et al.* [41, 42] prepared VPO

supported on TiO_2, Al_2O_3 and SiO_2; in this case an increased ethylene formation was observed, mainly related to a higher catalytic activity of the supported catalysts (especially on TiO_2) compared to the bulk catalyst. The enhanced performance was explained on the basis of a uniform dispersion of the active phase on the support, which leads to a higher surface area and enhanced reducibility. Recently, VPO catalysts supported on mesoporous materials based on an aerosil gel have demonstrated high yields to ethylene, higher than those obtained with supported samples synthesized by conventional methods [43].

In summary, relatively few studies on the oxidation of ethane using VPO catalysts have been published, and most of them have been limited to the use of catalysts consisting of a $(VO)_2P_2O_7$ phase prepared from a $VOHPO_4 \cdot 0.5H_2O$ precursor. Moreover, in most cases the surface characterization of the active materials, so important to understand the catalytic processes, has been limited to X-ray photoelectron spectroscopy (XPS), which, although providing average information from a few layers in the surface region of the catalyst, is not a "true" surface technique.

Accordingly, in the present paper, the study of undoped VPO catalysts based on the $(VO)_2P_2O_7$ phase for the ODH of ethane is further extended to other crystalline structures, such as $VOPO_4 \cdot 2H_2O$ and $VO(PO_3)_2$. The effect of different activation conditions for all the VPO structures, as well as the use of different precursors in some cases, is also studied. Moreover, the surface of the set of VPO catalysts has been systematically investigated at 400ºC by low energy ion scattering (LEISS) in addition to XPS, the former a characterization technique, which is sensitive only to the chemical composition of the outermost atomic layer. Comparison of the information obtained from both surface techniques has helped to

obtain a more complete and detailed picture of the catalysts surface at reaction temperature. This has enabled correlations to be made between the surface composition, the bulk structure and the catalytic performance of these materials for ODH of ethane.

Experimental

Preparation of the V-P-O precursors

The preparation of the **$VOHPO_4 \cdot 0.5H_2O$** precursor was conducted as follows: V_2O_5 and 85% H_3PO_4, with a V:P atomic ratio of 1:1, was refluxed (at 120 ºC) in isobutanol (250 ml) for 16 hours. Filtration was used to recover the solid formed which was washed in isobutanol (200 ml) and ethanol (250 ml). The resultant material was then refluxed at 100 ºC in distilled water for 3 h and filtered whilst hot. The final solid was dried in air at 120 °C for 16 h.

The **$VOPO_4 \cdot 2H_2O$** precursor was prepared by refluxing (at 120 ºC) V_2O_5 and 85% H_3PO_4, with a V:P atomic ratio of 1:1.2, in water (24 ml) for 8 hours. The solid was then recovered by hot filtration, washed with distilled water and dried in air at 110 °C for 16 h.

The preparation of the **$VO(H_2PO_4)_2$** precursor was conducted as follows: V_2O_5 and 85% H_3PO_4, with an excess of phosphorus (V:P atomic ratio of 1:10), were refluxed at 180 °C for 1 hour. Evaporation was used to recover the precipitate which was then washed with acetone and water to recover the excess H_3PO_4. The final solid was dried in air at 110°C for 16 h.

Preparation of the V-P-O catalysts

The catalyst named as **VP1** (mainly consisting of $(VO)_2P_2O_7$ phase) was prepared from $VOHPO_4 \cdot 0.5H_2O$ precursor. This precursor was heat-treated at 550 ºC for 3 h under a flow of 50 ml min^{-1} gas mixture of ethane/oxygen/helium with a molar ratio of 2/19/79.

The catalyst named as **VP1H** (mainly consisting of $(VO)_2P_2O_7$ phase) was also prepared from a $VOHPO_4 \cdot 0.5H_2O$ precursor, in this case activated in a He atmosphere (50 ml/min) at 550ºC for 3 h. VP1H was prepared as a variation of the VP1 sample to determine the influence of different activation conditions (reactive or inert atmosphere) on the same precursor, leading to the formation of a similar main bulk crystalline $(VO)_2P_2O_7$ structure.

The catalyst named as **VP2** (mainly consisting of $VOPO_4 \cdot 2H_2O$ phase) was prepared through the activation of the $VOHPO_4 \cdot 0.5H_2O$ precursor in static air at 550 ºC for 3 h.

The **VP3** catalyst was obtained from a $VOPO_4 \cdot 2H_2O$ precursor, which after activation at 550 ºC for 3 h in a 50 ml min^{-1} stream of ethane/oxygen/helium (2/19/79 molar ratio), led to a bulk $VOPO_4 \cdot 2H_2O$ structure similar to the precursor. **VP3** catalyst was prepared as a variation of the VP2 sample to determine the influence of using a different precursor to get a similar $VOPO_4 \cdot 2H_2O$ stabilized phase.

The catalyst named as **VP4** (mainly consisting of $VO(PO_3)_2$ phase) was prepared by the activation of $VO(H_2PO_4)_2$ precursor in 50 ml min^{-1} of a mixture of ethane/oxygen/helium (2/19/79, molar ratio) at 550ºC (for 3 h).

Finally, the catalyst named as **VP4H** (mainly consisting of a $VO(PO_3)_2$ phase) was obtained from the $VO(H_2PO_4)_2$ precursor (the same used to prepare the catalyst VP4), which in this case was activated in a He stream (50 ml min^{-1}) at 550ºC for 3 h. VP4H catalyst was prepared as a variation of the VP4 sample to determine the influence of different activation conditions (reactive or inert atmosphere) on the same $VO(H_2PO_4)_2$ precursor leading to the formation of a similar main bulk crystalline $VO(PO_3)_2$ structure.

Characterization techniques

Surface area was calculated from nitrogen adsorption-desorption isotherms (-196 °C) recorded on a Micromeritics ASAP-2020 automated analyzer. Samples were degassed for 5 h at 80 ºC and 10-6 Torr prior to analysis. Surface areas were estimated according to the Brunauer-Emmett-Teller (BET) model.

The particle size distribution has been determined by using a Malvern Mastersizer 2000 instrument equipped with a small volume sample dispersion unit. Ethanol was the dispersion media used. Each sample was measured in triplicate, accumulating light scatter data for 10 seconds (in each measurement as well as in the background). In order to favor the particle dispersion, samples were sonicated for 2 minutes at 15 watts in successive treatments until stabilization of the particle size distribution.

Powder X-ray diffraction employing a Bruker D8 Advance Series 2 diffractometer with a CuK_{α} source operated at 40 kV and 40 mA was used to identify the crystalline phases present in the powder catalysts.

Diffuse reflectance UV–Vis spectra were collected on a UV-2600 Shimadzu equipped with a "Praying Mantis" attachment from Harrick. The sample cell was equipped with a heater unit, a thermocouple and a gas flow system for in situ measurements. The samples were dehydrated in situ, in dry air at 150ºC for 30 min.

Raman spectra were recorded at room temperature using a 514 nm laser excitation on a Renishaw Raman Spectrometer (''in via'') with a CCD detector. The laser power employed was 25 mW and 20 acquisitions were taken for each spectrum. In all cases analyses on different positions of the sample were recorded in order to check homogeneity (spectral resolution ~ 1μm).

X-ray photoelectron spectroscopy (XPS) and low energy ion scattering spectroscopy (LEISS) data were acquired on the catalysts at 400 ºC, using a custom-made UHV instrument, at the Center for Functional Nanomaterials in Brookhaven National Laboratory (U.S.), equipped with a SPECS

PHOIBOS 100 MCD spectrometer, and specially design for isothermal in situ studies employing both techniques on site. No thermal treatment in O_2 was carried out for any of our VPO samples, inside the UHV chamber, prior to the XPS or LEISS analyses.

XPS data were collected using non-monochromated Al Kα (hν= 1486.6 eV) X-ray radiation at 300 W (15 keV and 20 A). Spectra were acquired with pass energy of 25 eV and energy step of 0.2 eV. The base pressure in the analysis chamber was kept below 5×10^{-9} mbar. XPS peak areas were calculated by integrating individual components after subtracting a Shirley background. Spectrometer transmission function, cross section and inelastic mean free path values from CasaXPS software were used for quantitative calculations.

The V($2p_{3/2}$) core level was used to determine the differences in the vanadium oxidation state among the VPO catalysts measured at high temperature (400 ºC), near the temperature range used for the catalytic reaction. The binding energy scale was calibrated to 530.0 eV for the O(1s) peak position as typically recommended for vanadium oxides [44-47] and especially for vanadium phosphorous oxides where the reference of C(1s) binding energy values are not reliable due to the uncertain chemical state of carbonaceous residues that mostly originate from the preparation involving organic solvent. The contribution of vanadium species in different oxidation states was estimated by curve fitting of the V($2p_{3/2}$) XPS peak using Gausian-Lorentzian profiles after Shirley background subtraction.

The low-energy ion scattering (LEISS) analyses were also performed at 400 ºC under UHV conditions, using He^+ ions with primary energy in the range of 1.0-1.5 keV. The angle of incidence of the He^+ beam with the sample surface was 45º, and the scattering angle was 135º. The ion

current, measured on the sample surface, was kept constant in the range 0.4-0.6 nA. Powder samples were compacted by mechanical pressure (0.5 Ton cm^{-2} for 1 min) to produce self-supporting pellets and to remove the macroscopic roughness. The self-supported sample pellets (*ca*. 15 mg) were thin enough to allow charge neutralization through a grounded metal support/sample holder. Ion scattering spectra were collected at low ion fluxes, in order to minimize any sputtering effects that could change and/or damage the sample surface. Except for the VP1H sample, all the samples showed clear and stable ion scattering signals from the very first scan, regardless of the presence of C in some of them. Unlike the rest of the samples, the first scans for VP1H at room temperature, using He^+ beam energies in the range of 1000-1500 eV, showed unstable signals at scattered energies close to the primary beam energy, causing detector saturation. After two sweeps at 1000 and 1500 eV He^+ beam energies, the catalyst surface was free enough from contaminants in order to show coherent LEISS spectra. A negligible sputtering effect on V and P species was confirmed by consecutive ISS scans showing insignificant changes on the surface composition after each scan.

Only the P/V atomic ratios were calculated, multiplying the P/V integral intensity ratio by the relative sensibility factor between vanadium and phosphorous LEISS signals. This factor has been determined as $F_{(V/P)} = 3.7$ by Delichère *et al.* using the "Dual Isotope Surface Composition" method which is based on the comparison of LEISS signals recorded with two different isotopes, $^3He^+$ and $^4He^+$. Since this method does not involve any calibration using reference patterns, the value provided is independent of errors due to influence of roughness and wrong assumptions of surface atomic densities of reference patterns.

Catalytic studies

The oxidation of ethane was carried out at atmospheric pressure, in the 300 to 500 ºC temperature range using a fixed bed quartz tubular reactor (20 mm inner diameter, 400 mm length). The feed consisted of a mixture of C_2H_6/O_2/He with molar ratios of 10/5/85. Several catalyst masses (from 0.05 to 2.5 g) and total flows (from 20 to 150 ml min^{-1}) were employed in order to obtain different contact times and comparative iso-conversion conditions among catalysts. Particulate catalyst samples (0.3 to 0.6 mm) were diluted with inert silicon carbide (0.6- to 1-mm particle size) in order to keep a constant volume for the catalytic bed. In order to achieve an even distribution of the active material and the diluent, the amount of catalyst loaded was divided into 4 portions and the same was done with the SiC. One portion of SiC was mixed with one portion of catalyst and the mixture was then added to the reactor. The same procedure was repeated for the remaining 3 portions. Prior to the first analysis, the catalyst was left stabilizing under the reaction conditions for 30 min.

Reactants and products were analysed by on-line gas chromatography using two packed columns: i) Molecular sieve 5Å (2.5 m), and ii) Porapak Q (3 m). Blank reaction experiments with no catalyst in the reactor tube showed no conversion at a reaction temperature of 500 ºC. In all cases carbon balances were 100 ± 4%, irrespective of the catalyst type and mass used.

Each data point for catalyst performance was determined by averaging two different analyses of reactants and products (ca. 15 min each). The differences were minor and indicated steady state was achieved. Additionally, the VP1 catalyst was selected to study catalytic performance with time on line for 5 h, maintaining the same reaction conditions, in order to check the catalytic stability of one representative VPO sample. No appreciable differences in either conversion or selectivity to ethylene were observed over this time period.

Results and Discussion

General characterization

Table 1 lists the precursors and the activation conditions used to prepare the VPO catalysts, as well as the main characteristics of the corresponding activated solids obtained, such as the major crystalline phases detected by XRD and the BET surface areas. The XRD patterns of the precursors employed, as well as those of the activated catalysts, are shown in Figures 1 and 2, respectively. Catalysts VP1 and VP1H, prepared from the same precursor but with different activation conditions (Table 1), present the same major $(VO)_2P_2O_7$ phase and similar specific surface areas of 9 and 15 $m^2\ g^{-1}$, respectively. Catalysts VP2 and VP3 show similar diffraction patterns typical of the $VOPO_4.2H_2O$ phase, despite the fact that they have been prepared using different precursors (Table 1). Nevertheless, a difference of crystallinity can be observed comparing both XRD results (Figure 2), as VP2 shows a pattern indicative of a less crystalline structure. According to this, VP2 presents a specific surface

area, 2.8 m^2 g^{-1}, which is significantly higher than that of 0.4 m^2/g observed for the VP3 sample (Table 1). Similarly, VP4 and VP4H catalysts, which mainly consist of $VO(PO_3)_2$ structure as indicated by their XRD patterns, also present very low specific surface areas which do not exceed 1-2 m^2/g, according to previous reports [48].

All the V-P-O samples present very low surface area. In fact, there is only significant adsorption at partial pressures near $P/P_0 = 1$. This indicates that the material is not porous (as expected), and the surface area measured by the N_2 adsorption technique corresponds only to the surface of the grains of the different catalysts. We want to note that in the adsorption measurements of N_2, it is necessary to take into account the way the sample has been prepared. As it is degassed under vacuum and heated (high vacuum and 80° C), it cannot be ruled out that some water molecules weakly bound to the material are eliminated. This could affect mainly the samples with $VOPO_4.2H_2O$. It is possible that by removing water the $VOPO_4$ layers are stacked, with the consequent increase of the particle size and a decrease of the BET area (0.4 and 2.8 m^2/g). The Adsorption–desorption isotherms of VP1H and VP4H are shown in Supporting Information (Figure S1). It must be noted that the determination of the surface area through the BET method presents some inaccuracy for these materials with low area.

As the material is not porous and the surface area must correspond only to the surfaces of the grains, the particle size distribution of representative catalysts (VP1H and VP4H) has been studied by using a Malvern Mastersizer 2000 instrument equipped with a small volume sample dispersion unit (see more details in Experimental section).

The particle distribution of the pyrophosphate VP1H sample (largest BET area), is shown in Figure S2 (Supporting Information). Three different curves are plotted: i) the catalyst suspended in ethanol, ii) the sample after a first sonication and iii) the sample after a second sonication treatment. After the second sonication a stable distribution could be observed. There are maxima around 0.7, 10 and 100 microns, although the distribution is broad (there are particles larger than 100-200 microns and others smaller than 1 micron).

In Figure S3 (Supporting Information) the particle size distributions of representative V-P-O catalysts, which have been stabilized are compared. The sample VP4H, consisting of $VO(PO_3)_2$ structure with low surface area (1.9 m^2/g), presents three particle size populations at similar values to that of the VP1H sample, i.e. at 0.7, 10 and 90 microns. In this case there is a higher proportion of grains at ca. 100 microns. However, and in agreement with the highest surface area, in the VP1H catalyst (15.6 m^2/g) the maximum appears at 7-8 microns.

It must be pointed out that two of the synthesized precursors, $VOHPO_4 \cdot 0.5H_2O$ and $VO(H_2PO_4)_2$, were activated in helium (leading to VP1H and VP4H samples respectively), or in a mixture of ethane/oxygen/helium, (leading to VP1 and VP4 samples respectively). Apart from the different crystallinity observed in the XRD patterns (Figure 2), the main phase obtained in each case was only dependent on the precursor regardless of the activation conditions. Thus, the $VOHPO_4 \cdot 0.5H_2O$ precursor leads to formation of $(VO)_2P_2O_7$ (VP1 and VP1H), while the $VO(H_2PO_4)_2$ precursor leads to $VO(PO_3)_2$ (VP4 and VP4H).

The activated catalysts were also analyzed by DR-UV-Vis. (Figure 3). Despite the complexity of the spectra obtained, as they consist of several broad and overlapping bands, complementary information can be extracted from them. Thus, a strong band at 200-250 nm (associated with a charge transfer transition from O^{2+} to V^{4+}) and a weak band at 600-650 nm, both found in VP1, VP1H, VP4 and VP4H samples, indicate the presence of V^{4+} species [49-54] which is in agreement with the expected vanadium oxidation state of $(VO)_2P_2O_7$ (in VP1 and VP1H catalysts) and $VO(PO_3)_2$ (in VP4 and VP4H catalysts). However, while the band at 600-650 nm is more specific to V^{4+}, and therefore barely observed in the samples with a major V^{5+}-containing VPO structure (VP2 and VP3 catalysts), absorption at 200-250 nm has also been related to isolated V^{5+} species in tetrahedral coordination. Moreover, a band at *ca*. 300 nm has been reported to be due to polymeric V^{5+} in tetrahedral coordination [49-54]. Accordingly, absorption within the region 200-300 nm is clearly present in the VP2 and VP3 catalysts spectra as well, both samples consisting of a V^{5+}-containing bulk phase ($VOPO_4.2H_2O$). With respect to the latter phase, the structure of which mainly consists of hexa-coordinated V^{5+} species, an absorption band at 400-450 nm has been reported to be related to those V^{5+} species [49-54]. This is also observed in VP2 and VP3 spectra, although with a strong difference in the relative intensity between both samples. Whilst VP3 presents an intense absorption maximum centred at 400-450 nm, a shoulder is barely observed instead in the VP2 sample within the same range, showing a similar intensity to that found for VP1 and VP1H samples mainly consisting of V^{4+}-containing structure. The lowest absorption at 400-450 nm is observed for VP4 and VP4H catalysts which accordingly are the only ones with no V^{5+} species found near the surface by XPS, as will be discussed later in detail.

The UV absorption at lower wavelengths within the 300-400 nm range observed for all samples is especially intense in VP2 and VP3 spectra, where it is likely to be due to V^{5+} species with different coordination and/or aggregation. In fact, the intensity of the UV/Vis absorption centred at ca. 400 nm has been used to track the reduction (V^{5+} into V^{4+} or V^{3+}) and the reverse oxidation during operando experiments with VPO catalysts during selective oxidation of n-butane [54].

According to these results, it can be stated that although the valence and oxidation state of vanadium expected for the main VPO crystalline phase are present in the activated catalysts, evidence of different vanadium environments and oxidation states are also found in all the samples studied, confirming the presence of significant inhomogeneity as typically reported for VPO materials. With respect to the effect of using different precursors and/or different activation conditions, comparison between DR-UV-Vis spectra of catalysts based on the same crystalline phase obtained from the same precursor show slight differences regardless of the different activation conditions used. Thus, the spectra of $(VO)_2P_2O_7$ based catalysts (VP1 and VP1H) are almost identical (Figure 3), while just a small variation in the absorption intensity below 300 nm is observed for the $VO(PO_3)_2$ based ones (VP4 and VP4H). The strongest differences are found instead in the DR-UV-Vis spectra of the VP2 and VP3 catalysts both containing the $VOPO_4.2H_2O$ phase, although obtained using a different precursor.

Complementary, Raman spectra were collected for the most representative samples (Figure 4), in order to investigate the possible minority presence of non ordered phases, invisible for the XRD, which could be catalytically important. A few spectra were collected for each sample at

different locations, confirming a good homogeneity in all of them. Catalysts consisting of $(VO)_2P_2O_7$ based catalysts (VP1 and VP1H) show spectra with a high degree of disorder with broad peaks. These spectra show a main broad band centred at 928 cm^1, which can be attributed to asymmetric P-O-P stretches in the $P_2O_7^{2-}$ unit of $(VO)_2P_2O_7$. A shoulder centred at *ca.* 980 cm^1 has also been observed especially in the sample activated in helium (VP1H). This signal could correspond to $VOHPO_4.0.5H_2O$ impurity not yet transformed into vanadyl pyrophosphate. However, the presence of some other $VOPO_4$ phases (δ or α_{II}) cannot be completely ruled out. A low intensity band has been observed at 1180 cm^{-1} which can be related to the V-O-P stretches of $(VO)_2P_2O_7$ [55-58].

VP4 and VP4H catalysts present two main peaks at *ca.* 932 and *ca.* 967 cm^{-1}. The band at 967 cm^{-1} is characteristic of the P-O stretch of $VO(PO_3)_2$ whereas that at 932 cm^{-1} can be attributed to the P-O stretch of the $VO(H_2PO_4)_2$ precursor. Other low intensity bands at higher Raman shifts over 1100 cm^{-1} are observed. Bands between 1210 and 1260 cm^{-1} are assigned to $VO(PO_3)_2$ whereas that at 1146 cm^{-1} corresponds to the $VO(H_2PO_4)_2$ phase [55]. According to these results it seems that the complete transformation from $VO(H_2PO_4)_2$ to $VO(PO_3)_2$ has not taken place. These two phases present structural similarities and the shift from 932 to 967 cm^{-1} is due to the formation of $(PO_3)_n$ chains in the $VO(PO_3)_2$ phase [55]. The bands at 932 cm^{-1} and 1146 cm^{-1} present higher relative intensity in VP4 than in VP4H, which indicates that the $VO(H_2PO_4)_2$ has developed to a higher extent into $VO(PO_3)_2$ when heat treated in hydrogen (VP4H) than when activated in ethane/air (VP4).

Oxidative dehydrogenation of ethane

The different VPO catalysts were tested for the oxidative dehydrogenation of ethane. Ethylene and carbon oxides were the only reaction products observed in all cases (Table 2), and no traces of acetic acid or other oxygenated compounds were detected. Figure 5a shows the evolution of the ethane conversion with the reaction temperature for the VPO catalysts using the same contact times in all cases. As it can be observed, VP1 and VP1H catalysts, both comprising the $(VO)_2P_2O_7$ phase, provide a similar high catalytic activity, whereas ethane conversion is low for VP4 and VP4H catalysts, which are based on the $VO(PO_3)_2$ structure. For the VP3 sample, which consists of a $VOPO_4.2H_2O$ bulk phase, the ethane conversion is scarcely detectable, even at the highest reaction temperatures employed. Surprisingly, VP2 is remarkably more active than VP3 although both catalysts present the same major crystalline phase, $VOPO_4 \cdot 2H_2O$. However, it has to be noted that a significantly higher surface area was measured for VP2 compared to VP3 (Table 1).

If the surface area of the catalysts is taken into account to determine the catalytic activity the behaviour observed is different (Figure 5b). Most of the catalysts show a similar trend; only the VP3 sample shows an areal rate considerably lower than the average of the other catalysts.

Figure 6 shows the variation of the selectivity to ethylene as a function of ethane conversion on the different VPO catalysts under isothermal conditions (500ºC), using the same ethane/oxygen/helium feed ratio, but different contact times (changing either catalyst mass or total feed flow). The most selective catalysts are VP4 and VP4H, containing $VO(PO_3)_2$ as the major phase, with both showing a selectivity to ethylene close to

90% at 10% ethane conversion. This selectivity is much higher than that of 65-75% obtained at similar conversions with the VP1 and VP1H catalysts, which are based on a conventional $(VO)_2P_2O_7$ phase. It has to be mentioned that the catalytic performance observed for VP1 and VP1H is similar to that previously reported in the literature for ethane ODH with conventional $VO_2P_2O_7$ based catalysts [34-43]. The higher selectivity to ethylene obtained with samples containing $VO(PO_3)_2$ compared to those containing $(VO)_2P_2O_7$ is not evident at conversions close to zero, as all these catalysts present an initial selectivity very close to 100%. However, as the ethane conversion increases, the ethylene formed is significantly more reactive over the catalysts based on $(VO)_2P_2O_7$ than with those based on $VO(PO_3)_2$, thus lowering the selectivity of the former ones. It must be indicated that although the catalysts containing the $VO(PO_3)_2$ phase appear as the most selective to ethylene, the catalytic activity is low, and so is the ethylene productivity per mass unit of catalyst. In fact, contact times 15 times higher than with $(VO)_2P_2O_7$ based catalysts must be used to achieve similar conversions (Table 2).

On the other hand, the VP2 and VP3 catalysts based on the $VOPO_4 \cdot 2H_2O$ phase were remarkably less selective to ethylene than those containing $VO_2P_2O_7$ or $VO(PO_3)_2$ structures (Figure 6). For both VP2 and VP3 catalysts initial selectivity to ethylene below 90 % was observed. In the case of VP2, the selectivity to ethylene drastically decreases as increasing the ethane conversion, and just 30% selectivity to ethylene is obtained at *ca.* 12% ethane conversion. Due to the lower catalytic activity of VP3, for which conversions higher than 2% were not achievable even for long contact times, it was not possible to obtain further selectivity data.

At this point it should be mentioned that unlike the significant differences observed in the catalytic behaviour of $VOPO_4 \cdot 2H_2O$ based catalysts (VP2 and VP3), which were obtained from both different precursor and activation conditions, only slight differences were found between the rest of the VPO catalysts comparing samples containing the same major phase, but obtained from different activation conditions from the same precursor. Thus, for the VP1 and VP1H samples containing $VO_2P_2O_7$, the activation of the corresponding precursor in helium leads to a slightly more active catalyst (VP1H) than activation in a C_2H_6/O_2/He mixture (VP1), while the opposite was observed in terms of selectivity to ethylene. Likewise, even smaller differences in terms of both catalytic activity and selectivity to ethylene were found comparing VP4 and VP4H catalysts, whose primary $VO(PO_3)_2$ phase is formed from the same activated precursor, similarly to the VP1-series, either in a C_2H_6/O_2/He mixture or He.

Surface characterization

VPO catalysts, especially those with a $(VO)_2P_2O_7$ bulk phase, have been typically reported to show dynamic surfaces with a structure different from the bulk [59]. In order to investigate these differences, the chemical composition and electronic structure near the surface (averaged up to ~50 Å depth) at 400 ºC have been probed by X-ray photoelectron spectroscopy (XPS) on the most representative VPO catalysts prepared in this study, i.e. VP1H, VP2, VP3 and VP4H. In addition, the same catalysts were also analyzed at 400 ºC by low energy ion scattering spectroscopy

(LEISS) to obtain information about the chemical composition of the outermost atomic layer, which is directly involved in the catalytic processes taking place at the solid-gas interface.

XPS results indicate that the phosphorus/vanadium atomic ratios for VP1H, VP2 and VP3 catalysts are higher (P/V between 1.3-2.0) than those corresponding to the stoichiometry of the respective bulk phases (P/V of 1.0), i.e. $(VO)_2P_2O_7$ for VP1H or $VOPO_4 \cdot 2H_2O$ for VP2 and VP3 (Table 3). Nevertheless, the values are within the range typically reported for this class of materials [33,60], for which an elevated P/V ratio is usually explained by a higher amount of surface terminal (pyro)phosphate groups [61-63]. Conversely, the VP4H catalyst shows a significantly higher P/V ratio of >4 (Table 3), which is in agreement with the surface P/V ratio (4.0) found in the literature for the $VO(PO_3)_2$ phase [63-65]. The metaphosphate $VO(PO_3)_2$ phase has been reported to be formed upon thermal pre-treatment of a $VO(H_2PO_4)_2$ precursor [63-66], which is indeed the precursor phase used in the VP4H sample prior to the activation treatment at high temperature (Table 1). The fact that the near surface vanadium/oxygen ratio observed by XPS for the VP4H catalyst (V/O of 0.06-0.07) is lower than that for the rest of the catalysts (V/O between 0.10-0.15), while phosphorus/oxygen ratios remain constant (P/O ~ 0.25) for all of them, indicates that the higher P/V ratio observed for VP4H is due to vanadium depletion near the surface rather than an excess of phosphorus (Table 3). This is in agreement with the model proposed by Delichere *et al.*, who argued that the high experimental P/V ratios are the result of vanadium vacancies in the amorphous surface layers of VPO catalysts [63,66]. The surface oxygen content determined by XPS (Table 3), is slightly higher (66 %) in the VP3 catalyst compared to the rest of

the catalysts (55-57 %), which is in agreement with the highest oxidation state of vanadium found at the near surface of VP3 (Table 4), as will be discussed more in detail later.

The highest near surface oxygen content for VP3 is also consistent with the lowest amount of carbon deposited on this catalyst, around 10 % at., compared to approximately double amount of carbon found on the rest of the catalysts (Table 4), all of them measured by XPS at 400ºC in ultra-high vacuum conditions. Usually a relatively high carbon content has been reported for vanadium phosphorous oxides measured at room temperature [62,65-67]. The carbon accumulation on the surface of VPO catalysts has been typically related to a loss of oxygen or its restricted availability from the lattice [68].

With respect to the near surface vanadium electronic structure, strong similarities were unexpectedly found between VP1H and VP2 catalysts, which despite sharing the same precursor ($VOHPO_4 \cdot 0.5H_2O$), present distinct bulk structures with different vanadium oxidation states, i.e. V^{4+} and V^{5+} for VP1H and VP2, respectively. Thus, $V(2p_{3/2})$ XPS spectra of both VP2 and VP1H catalysts can be fitted to three peaks with binding energies of 516.7, 515.7 and 514.5 eV, which we assign to V^{5+}, V^{4+} and V^{3+} species, respectively (Figure 7). With respect to V^{5+} and V^{4+} species, they have been typically reported at slightly higher binding energies in VPO catalysts used for n-butane partial oxidation [66-71]. Nevertheless, 516.7 and 515.7 eV are within the typical values reported for V^{5+} [67-72] and V^{4+} [44,72,73] oxides, respectively. A $V(2p_{3/2})$ binding energy of 516.7 eV also can be found in pure V^{5+} phosphorus oxides [67,74]. V^{3+} species are not usually reported to be present in fresh VPO catalysts, but

some studies make reference to them after partial vanadium reduction under reaction conditions [71]. Binding energies for either V^{3+} phosphorus oxides or pure V^{3+} oxides are usually reported at values in the range 515.0-515.6 eV; higher than those observed at 514.5 eV here [44,71,72,75]. The shift to lower binding energy has been related to V^{3+} bound to O-H, O-C or nitrogen [44,71,72,75].

The V^{4+} peak at 515.7 eV represents the main contribution of the total V($2p_{3/2}$) signal for both VP2 and VP1H catalysts, with 72 % and 43 % respectively (Table 4). Contrary to the expectations, the V^{5+} near surface content of the VP1H sample (consisting of a bulk V^{4+} phase) is slightly higher than that in VP2 (mainly containing a V^{5+} amorphous phase), while the opposite occurs for the V^{4+} content. However, the average oxidation state of near surface vanadium is higher in the VP2 catalyst (+4.1) compared to the VP1H (+3.9), since the amount of V^{3+} in the latter is three times higher.

The accuracy of the curve fitting results and the assignment of oxidation states was confirmed by comparison with the average oxidation state of vanadium calculated from the relation between the vanadium oxidation state and the splitting between O(1s) and V(2p3/2) transition centroids (Table 4) [46]. The relationship was found by Coulston and coworkers in VPO materials, and it is described as:

$V_{ox} = 13.82 - 0.68\ [O(1s) - V(2p_{3/2})]$

This equation is known as the Coulston equation and it is typically used to calculate the average oxidation state of vanadium from XPS analyses in VPO samples [46, 49, 66].

The curve fitting of the V($2p_{3/2}$) XPS peak at 400 ºC for the VP3 catalyst (with a bulk phase consisting purely of V^{5+}, $VOPO_4 \cdot 2H_2O$) is consistent with the presence of *ca*. 20 % of V^{5+} and 80 % V^{4+} species with binding energies at 516.7 and 515.7 eV, respectively (Figure 7, Table 4). Stoichiometric V^{5+} phosphorus oxide phases such as α_{II}-$VOPO_4$ should only contain V^{5+}, however they are typically reported as containing both V^{5+} and V^{4+} surface species with binding energies at *ca.* 518.2 and 516.7 eV correspondingly [67,74]. The lower binding energy for V^{5+} and V^{4+} species found here, compared to other work on VPO catalysts [66-70], is most likely related to vanadium being bound to oxygen-carbon. This is in agreement with the significant amount of carbon detected on the surface of these catalysts (Table 3). In fact, both 518.2 and 516.7 eV vanadium binding energies have been reported for α_{II} -$VOPO_4$ and β'-$VOPO_4$ (V^{5+}-containing phases) prepared with organic solvent [67]. However, only a peak with a binding energy of 518.2 eV is found for a β'-$VOPO_4$ phase prepared in aqueous solution [67]. In our case, the assignment of 516.7 eV to V^{5+} and 515.7 to V^{4+} (as used already for VP2 and VP1H) gives rise to an average vanadium oxidation state of +4.2, which is again consistent with that obtained from the difference between the O(1s) and V($2p_{3/2}$) binding energies by applying the Coulston equation [46,49-51,66] (Table 4). The VP3 catalyst is the only one with no V^{3+} component from the XPS analysis and the highest average near surface vanadium oxidation state, which is in agreement with the highest near surface oxygen content in comparison to the other VPO catalysts (Table 3).

Finally, the V($2p_{3/2}$) core level spectrum of the VP4H catalyst (Figure 7, Table 4) mainly consists of V^{4+} species (84 %) with a minor contribution of V^{3+} bound to O-C or O-H [44,71,72,75], and is the only one showing no V^{5+} component. This result is consistent with the V^{4+} phosphorus oxide forming the bulk of this sample, i.e. the $VO(PO_3)_2$ phase. This is consistent with the DR-UV-Vis spectrum of the VP4H catalyst showing the highest intensity for V^{4+} related bands, while the lowest absorption in the V^{5+} region (Figure 3).

LEISS analyses were performed on the same VPO catalysts investigated by XPS in order to probe the relative composition of the outermost atomic layer (Figure 8) and compare the results with the average chemical composition in the near surface region. The VP2 catalyst, activated in air at 550 ºC and consisting of an amorphous V^{5+}-containing bulk phase ($VOPO_4 \cdot 2H_2O$), shows a LEISS spectrum with clear and stable ion scattering signals corresponding to O, V and P from the very first scan at 400 ºC (Figure 8, b). Data were collected under steady state conditions (i.e., no desorption from the catalyst, with background pressure in the 10^{-9} mbar range). Vanadium and oxygen are the main peaks with a V/O signal intensity ratio of *ca*. 1, while that of P/O is about 2-3 times lower (Table 5). Moreover, the phosphorous peak has a broad shape and a long low-energy tail consistent with a signal controlled by re-ionization of the primary He^+ ions. This is most likely coming from slight penetration into the outermost exposed surface of the rough solid, suggesting a location of phosphorous species at 2-3 layers thick surface dimple defects [76]. A less intense but qualitatively analogous LEISS spectrum is found for the catalyst VP3 (Figure 8, c), which is in agreement with a similar

$VOPO_4 \cdot 2H_2O$ crystalline phase detected. Thus, V/O intensity ratio in VP3 is also close to 1, although the P content in the outermost layer (P/O intensity ratio of 0.15) is half of that found on the VP2 catalyst (Table 5).

LEISS spectra of the $VOPO_4 \cdot 2H_2O$ phase in VP2 and VP3 samples resemble those typically reported for equilibrated VPO catalysts consisting of $(VO)_2P_2O_7$, although the latter ones usually show an oxygen signal significantly higher compared to V or P, with lower V/O intensity ratios [66,69,77]. The V/O ratios, reported for $(VO)_2P_2O_7$, only reached a value close to 1 after a significant number of scattering cycles gradually sputtering the surface [66]. At this point it has to be mentioned that, to the best of our knowledge, no LEISS spectra of a $VOPO_4 \cdot 2H_2O$ phase have been reported so far, and those here presented (i.e. VP2 and VP3 samples) were collected at 400 ºC on a fresh sample with no previous sputtering cycle.

Unexpectedly, the VP1H catalyst, which does consist of a $(VO)_2P_2O_7$ bulk structure, shows a LEISS spectrum at 400 ºC consistent with an outermost atomic layer mostly containing V atoms, with a meaningless P signal (Figure 8, a). This LEISS spectrum is completely different to those previously reported for conventional $(VO)_2P_2O_7$ phases at room temperature [48,50,58], and also different to the rest of the VPO samples studied here at 400 ºC. Unlike the VP2 and VP3 catalysts, first LEISS analyses of VP1H, using He^+ beam energies in the range of 1000-1500 eV, provided unstable signals at scattered energies close to the primary beam energy (not shown), causing detector saturation and incoherent spectra. This was an indication of surface contamination (likely favoured by the activation step in He instead of oxidizing conditions), which makes

charge neutralization difficult and causes a positive surface charging voltage that prevents He^+ ions from reaching the sample. Instead, He^+ ions are reflected toward the detector at roughly the same primary kinetic energy [76]. After two sweeps at 1000 and 1500 eV He^+ beam energies, the catalyst surface became clean enough to show a coherent LEISS spectrum (Figure 8, a). However, inhomogeneous charging of the catalyst surface is still present and most likely responsible for the significant shifting of the vanadium peak to a kinetic energy higher than the theoretical value. The VP1H catalyst shows the highest vanadium content in the outermost surface, from among all VPO phases here studied at 400 ºC (Table 5). That is contrary to the trend observed near surface by XPS results at identical measurement conditions, where the second highest P/V atomic ratio is obtained for the VP1H sample, with an amount of P twice the amount of V.

The VP4H catalyst consisting of a V^{4+} bulk phase, $VO(PO_3)_2$, displays a LEISS spectrum (Figure 8, d) with a large amount of C. Similarly to the VP1H, the VP4H catalyst was also activated in a He stream, which is consistent in both cases with a high surface contamination compared to the VP2 and VP3 catalysts activated under oxidizing conditions. In order to confirm the peak assignment on the VP4H catalyst, LEISS was also performed using 1500 eV He^+ ions (Figure 8, d'). At this higher primary energy, the ion yield and resolution for O, P, and V signals increased and the kinetic energies, although still shifted, approached the theoretical values (which are He^+ primary energy dependant). In addition, the C peak disappeared in the 1500 eV LEISS spectrum, showing instead an increased background below 400 eV (likely due to ionization and sputtering of unstable C species weakly bond to the catalyst surface). The V/O intensity ratio in the LEISS spectrum of VP4H is the lowest compared to the

rest of the catalysts, which leads to the highest P/V intensity ratio approaching to 1 (Table 5). That is qualitatively in agreement with the highest P/V atomic ratio found in XPS for this sample (Table 3).

It is important to remind that, until now, only integral intensity ratios of LEISS signals have been discussed. Therefore, the comparison between LEISS and XPS results so far has been only qualitative, and limited to the relative trend observed among the different VPO phases studied. Quantification of relative atomic concentrations from the yield of scattered ions measured in LEISS, depends on elemental sensitivity factors. Those factors are difficult to determine, mostly due to the not straightforward task for preparing reference patterns with well known structure of the outermost atomic layer. As already mentioned with more detail in the experimental section, an alternative method, "Dual Isotope Surface Composition", which does not require of reference patterns, has been used by Delichère *et al.* to provide a sensitivity factor of 3.7 for the LEISS signal of V relative to P [66]. By using that sensibility factor we have estimated the P/V atomic ratios on the outermost surface of our VPO samples (Tabla 5), in order to compare them with those obtained from XPS. Thus, P/V atomic ratios from LEISS are lower than those from XPS in all VPO samples, which indicates an enrichment of V in the outermost atomic layer compare to the near surface composition. This V-enrichment is maximum in the case of VP1H sample based on $(VO)_2P_2O_7$ phase, and contrary to what has been reported so far for VPO catalysts containing the same phase [66, 69, 77]. In this sense, we have to consider that our $(VO)_2P_2O_7$ based sample has been measured at 400 °C, while most of the LEISS studies have been performed at room temperature. The "true" surface of VPO based materials, especially those containing

$(VO)_2P_2O_7$, has shown to be a quite dynamic system where the chemical composition is strongly and easily influenced by the temperature, and the pressure and nature of the gas-phase in contact with the surface. As an example of this, P/V atomic ratios of 4 or 2.4 were obtained by LEISS for a $(VO)_2P_2O_7$ based sample at 200 or 500 °C, respectively, at a certain partial pressure of water [77]. There are also studies where P/V atomic ratio from LEISS change from 2.0 to 3.9 for the same equilibrated $(VO)_2P_2O_7$ sample cleaned (carbon removed with an oxidation treatment in O_2 at 573K) or after being transported through air, respectively [69].

To the best of our knowledge, none of the LEISS P/V ratios reported have been measured under the same conditions (mainly temperature and vacuum pressure) used in our work, despite the fact that none of the works providing LEISS P/V ratios used the same preparation conditions for the $(VO)_2P_2O_7$ based sample that we employed. To all this, it has to be added the differences in the pre-treatment of the sample before the LEISS measurements. Some works, run some sputtering cycles, others make an oxidizing treatment at high temperature. Moreover, different ion currents used during the LEISS measurements can modify the surface termination by contributing differently to the surface sputtering. In this sense, we used an extremely low ion current within the 0.6-0.4 nA range, to avoid any sputtering and so modification of the pristine surface termination. This ion current is much lower than that found in any of the papers using LEISS on VPO, where the lowest current found was 27 nA [77], and the highest 50 nA [66]. Due to all aforementioned, comparison between P/V atomic ratios among different works has to be taken carefully and with full knowledge of the facts.

Relationship between VPO bulk phase, near and outermost surface features and the catalytic performance

The catalytic performance observed for the different VPO catalysts cannot be explained in terms of a single factor, but from a combination of their bulk and surface features. In this sense, strong differences are found in the chemical composition and electronic structure of vanadium between the bulk and the surface of these vanadophosphate catalysts, as well as in the composition of their outermost atomic layer, which definitely do not extend further into the near surface region. Thus, the results obtained by LEISS, only sensitive to the outermost atomic layer, show important differences compared to those obtained by XPS which, although a surface sensitive technique as well, offers average information of up to ~5 nm deep into the solid for the kinetic energies used in our study. This fact reinforces that it is appropriate to investigate the outermost surface of a catalyst in order to provide further understanding on the catalytic processes. In the case of the $VO(PO_3)_2$ phase (VP4H catalyst), the relative amount of phosphorus on the surface, with respect to vanadium is the highest amongst the VPO phases studied, while the V/O ratio is the lowest observed, either near surface by XPS or outermost atomic layer by LEISS. Considering that vanadium is mainly responsible for the hydrocarbon activation, the low surface vanadium content may explain the low activity achieved on the VP4H catalyst consisting of a $VO(PO_3)_2$ phase. Indeed, the metaphosphate $VO(PO_3)_2$ phase (contained in VP4H) has also been reported to show poor activity for partial n-butane oxidation [33,60]. Nevertheless, the $VO(PO_3)_2$ phase shows the highest selectivity to ethylene for ethane oxidation, compared to the rest of the

phases studied here. Thus, VP4H and VP4 catalysts containing a $VO(PO_3)_2$ phase have been the only ones reaching 100 % selectivity at initial ethane conversion (Figure 5), which indicates an exclusive transformation of ethane into ethylene with absolutely no contribution of the reaction pathways leading to carbon oxides formation from ethane, or ethylene decomposition, as shown in the reaction scheme (Figure 9A). In this sense, the site isolation principle, reported for n-butane oxidation on VPO catalysts [21], could also be applied to explain the remarkably higher selectivity to ethylene observed for the $VO(PO_3)_2$ phase, in which the surface vanadium active sites would be the most isolated, according to the higher P/V atomic ratio by XPS, and higher P/V signal intensity ratio by LEISS, compared to the other VPO catalysts. Moreover, unlike the others, this $VO(PO_3)_2$-containing sample (catalyst VP4H) shows a high content of apparently stable carbonaceous species in the outermost surface at 400 °C in UHV conditions (Fig. 7). It cannot be ruled out that the carbonaceous species still remain under reaction conditions blocking highly active V sites leading to ethylene decomposition, and so contributing to the isolation of V sites less active and more selective to the olefin formation.

In the case of the catalyst VP1H containing $(VO)_2P_2O_7$ phase, the vanadium amount in the near surface is twice that for VP4H (Table 3). VP1H shows the highest catalytic activity, although its near surface vanadium content is not higher than in other much less active catalysts, i.e. VP2 and VP3. Nevertheless, the highest vanadium content in the outermost atomic layer of the catalyst VP1H, with phosphorus not even appearing in the LEISS spectrum (Figure 8), would explain its higher catalytic activity. Although vanadium has been reported as the main active site for

hydrocarbon oxidation in VPO catalysts [34-43], this statement has to be made with caution since other parameters, may also play an important role in addition to the amount of vanadium on the surface. In fact, the catalytic activity for ethane oxidation seems to be strongly related to the surface area of the V-P-O catalysts studied (Tables 1 and 2). However, this discussion is complicated as the surface areas of the VPO catalysts are very low in all cases and the inaccuracy of the BET method, high in these cases.

On the other hand, the oxidation states of vanadium can also play an important role in both, the type of ethane activation (selectivity to the olefin or to CO_x) and the ethylene decomposition. Figure 9a shows a proposed reaction scheme for ODH of ethane on VPO catalysts, where two pathways leading to carbon oxides are proposed: i) directly from unselective ethane oxidation, and ii) as secondary products from overoxidation of ethylene. In this sense, it is known that V^{5+} strongly adsorbs negatively charged olefin-like intermediates, and these favour the unselective oxidation of ethylene into CO and CO_2 [37]. Accordingly, our results indicate that the least selective catalysts are those consisting of a crystalline phase ($VOPO_4 \cdot 2H_2O$) with +5 oxidation state of vanadium, *i.e.* VP2 and VP3, whereas the most selective catalysts correspond to those containing crystalline phases with an oxidation state of +4 for vanadium, i.e. VP1H and VP4H, with $(VO)_2P_2O_7$ and $VO(PO_3)_2$ structures, respectively. Indeed, it is observed that the lower selectivity to ethylene for the catalysts with V^{5+}-containing phase (VP2 and VP3 samples) is the result of a higher decrease of the selectivity to ethylene with the ethane conversion, which indicates a higher extent of olefin decomposition into carbon oxides, according to the reaction scheme of V-P-O catalysts for ethane oxidation displayed in Figure 9a. As it can be seen, the initial

selectivity to ethylene (at conversions near zero) is for all VPO catalysts very high; however the decrease in selectivity with conversion is more important for those catalysts with a V oxidation state of +5.

Coherently, the catalyst VP4H, with the highest selectivity to ethylene, shows no V^{5+} species in the near surface region under the measurement conditions (Table 4), i.e. at 400ºC in ultra-high vacuum. The existence of V^{5+} in the VP4H cannot be discounted under reaction conditions due to a partial surface reoxidation with molecular oxygen from the reaction feed.

Unexpectedly, the amount of V^{5+} found by XPS for the VP1H catalyst (23%), the next one below VP4H in selectivity to ethylene, is slightly higher than that for the VP2 (17%) and VP3 (21%), which are catalysts more prone to ethylene decomposition. However, VP1H shows the highest surface content of V^{3+}, which is three times lower in VP2, twice lower in VP4H, and is absent for VP3. Thus, although V^{4+} near surface in VP2 and VP3 (containing V^{5+} phase) is also unexpectedly higher than that for VP1H (containing V^{4+} phase), the mean vanadium oxidation state of 4.1-4.2 in the former ones is above that for the VP1H (3.9-4.0). Indeed, the lowest value for the mean oxidation state of V (3.8-3.9) is found in the catalyst VP4H hardly active for ethylene decomposition (Figure 9).

At this point it must be mentioned that V^{3+} has been reported to be frequently present as defects in phases of VPO catalysts used for n-butane selective oxidation [54,60,68]. The density of V^{3+} defects, mostly generated during the thermal treatment of the precursor, depends on the amount of organic residues retained in the precursor and the nature of the heat treatment carried out for the transformation of the precursor into the active

catalyst [21]. Formation of V^{3+}, through V^{5+} and/or V^{4+} reduction, has also been described in VPO catalysts under reaction conditions of low oxygen partial pressure during n-butane selective oxidation [21,58,64]. That reduction was found to be accompanied by a release of lattice oxygen from the catalyst framework and the formation of surface carbon deposits. Indeed, the catalyst with the lowest amount of carbon near surface (sample VP3) is the only one without V^{3+} surface species (Table 4). It has to be noted that, regardless of the atmosphere of the activation method used (He, air or ethane/air), our fresh catalysts were measured at 400ºC in ultra-high vacuum conditions, i.e. a negligible oxygen pressure where any organic residue on the sample would act as a reducer removing oxygen atoms from the catalyst framework. In that sense, the formation of small VPO_4 local domains (a V^{3+} phase) cannot be ruled out in the catalysts where V^{3+} has been detected by XPS, since the loss of lattice oxygen has been reported as the first step in the epitaxial transformation of $(VO)_2P_2O_7$ to VPO_4 [68]. Anyway, slight partial reduction or oxidation of vanadium in VPO catalysts seems to have no significant effect on the long-range order of their crystalline domains, but rather local changes on the surface of small crystalline or amorphous domains, which are not accessible by X-ray diffraction characterization [54].

Although the selectivity to ethylene in the ethane oxidation on VPO catalysts might be favoured by the absence of V^{5+} species, our results suggest that what actually determines the selectivity to ethylene, rather than the absolute content of V^{5+} on the surface, is a suitable redox balance of vanadium favoured by an adequate amount of V^{3+} species, which seems to be strongly influenced by the nature of the bulk phase.

These results obtained for ODH of ethane with respect to V^{5+} surface content are partly contrary to what has been reported in some occasions for n-butane selective oxidation on VPO catalysts, where a defined amount of V^{5+} near surface is essential in order to get the highest selectivity to maleic anhydride [21]. In this sense, it is generally accepted that the selective oxidation of n-butane over $(VO)_2P_2O_7$ proceeds via a redox cycle between V^{4+} and V^{5+}, where n-butane reacts with the oxidized surface which transfer oxygen atoms, released from the catalyst framework, into the reactant molecules [78]. This process is accompanied by a reduction of V^{5+} to V^{4+} and, to a lesser extent, possibly even to the V^{3+} state. The catalyst vacancies formed are refilled by oxygen from the gas phase changing the oxidation state back to V^{5+}, as it would correspond to a catalytic cycle with a Mars-van-Krevelen mechanism [54]. The amount of active oxygen species corresponds to that of surface V^{5+} [78]. Therefore, the isolated V^{5+} surface sites are thought to be responsible for the activation of the n-butane and for the O-insertion.

Although the ODH of ethane also requires oxygen to form water from the dehydrogenation of the alkane, the reaction does not involve the insertion of oxygen into the reactant molecule, unlike the selective oxidation of n-butane. In addition the reaction from n-butane requires seven times higher the amount of oxygen according to the reactions stoichiometry. Hence a significantly different influence of V^{5+} in the catalytic performance of VPO catalysts should be expected between both reactions, as indeed has been observed.

On the other hand, the role of V^{3+} has been reported to be controversial for the selective oxidation of n-butane over VPO catalysts. Although a discrete number of V^{3+} species in the near surface the $(VO)_2P_2O_7$ lattice, and the associated anionic vacancies, have been proposed to play a

positive role on the catalytic activity, they have been found to be unfavorable for the selectivity to maleic anhydride [21,54,68]. On the contrary, V^{3+} surface sites appear essential for ODH of ethane in order to get the highest selectivity to ethylene and to avoid its decomposition due to undesired further oxidation under high conversion conditions.

It makes sense that a redox couple between vanadium species with lower reduction potential, i.e. less oxidizing power as compared to the optimal for n-butane oxidation, is needed to carry out the catalytic cycle for ethane oxidation through the consequent catalyst reduction, and catalyst re-oxidation with molecular oxygen. In this sense, an exclusive V^{3+}/V^{4+} couple appears to be the most appropriate, according to the highest ethylene selectivity reached over the VP4H catalyst, with a V^{3+}/V^{4+} ratio of 0.2 and no V^{5+} species found near the surface (Table 4). Nevertheless, a higher content of V^{3+} surface species seems to partially compensate the presence V^{5+}, in agreement with the high ethylene selectivity obtained for the VP1H catalyst, with V^{5+}/V^{4+} and V^{3+}/V^{4+} ratios of ca. 0.5 and 0.8, respectively.

Finally, we have shown that the phosphorus enrichment of the VPO catalysts surface, widely reported in the literature, is limited to the near surface at the measurement temperature here used (400 °C). Thus, an enrichment of vanadium takes place instead at the outermost atomic layer for all VPO phases investigated here, with negligible amount of phosphorous observed at 400 °C for the sample VP1H consisting of the $(VO)_2P_2O_7$ phase (Figure 8, a).

Summarizing, among the V-P-O phases here studied for the oxydehydrogenation of ethane, some phases are more active, such as $(VO)_2P_2O_7$), and other ones more selective to ethylene, such as $VO(PO_3)_2$. If the catalytic results obtained in the present work are compared to the most relevant reported in the literature (Table 6) it can be observed that VPO catalysts present a poorer performance in terms of catalytic activity and selectivity to ethylene than the catalysts of choice based on nickel oxide or MoV-bronzes. In Table 6 the specific activity per surface area is also included, $(VO)_2P_2O_7$ showing the highest areal rate. However, these data correspond to reaction temperatures higher than those used in the other catalytic systems.

In order to improve the catalytic performance of the V-P-O catalysts we could follow two approaches: i) try to increase selectivity in the most active catalysts or ii) increase the activity in the most selective catalysts. The preparation method of these catalysts has been shown as highly determining and could be further optimized [79]. For example, we could use supported vanadyl phosphate $VO(PO_3)_2$ structures with increased surface area. The activation conditions could also be modified, as it has been widely reported that activation drastically affects the catalyst structure and consequently the catalytic performance of $(VO)_2P_2O_7$) [80,81]. A kinetic study could also be useful to probe the reaction pathways and mechanism, this way permitting us to design more efficient catalysts.

Conclusions

A set of V-P-O phases have been tested in the oxidative dehydrogenation of ethane and their surfaces characterized by XPS and LEISS. A strong influence of the V content (relative to P), in the outermost surface, on the alkane conversion is confirmed by the highest and the lowest catalytic activity obtained for the lowest and the highest P/V signal ratio from LEISS analysis, respectively. Nevertheless, the catalytic activity for all VPO structures studied has shown a strong correlation with the specific surface area regardless of the VPO structure. Thus, the $(VO)_2P_2O_7$ based catalysts, with the highest surface areas and true surface vanadium contents, turned out to be the most active ones.

Regarding the selectivity to ethylene, the highest value is reached using $VO(PO_3)_2$ based catalysts, which have proved to be the most selective VPO catalysts reported so far for ethane oxidation at equivalent ethane conversion. The least selective catalysts have been those containing the $VOPO_4{\cdot}2H_2O$ phase, while the ones consisting of $(VO)_2P_2O_7$ showed an intermediate selectivity to ethylene..

The highest selectivity to ethylene obtained with a $VO(PO_3)_2$ based catalysts can be related to the most isolated V surface sites (revealed by the highest P/V LEISS signal ratio) in the most reduced oxidation state (3.8-3.9 averaged value from XPS) both found at 400 °C under UHV conditions, compared to the rest of catalysts. Unfortunately, $VO(PO_3)_2$ based catalysts show poor catalytic activity, leading to ethylene yields per mass unit of catalyst significantly lower than conventional $(VO)_2P_2O_7$ based catalysts. However, taking into account the relative content of vanadium atoms, considered as the active species, on the outermost surface of both $VO(PO_3)_2$ and $(VO)_2P_2O_7$ containing catalysts, turnover frequencies on the former would be *ca.* 20 times higher than on the latter ones. These promising results encourage further investigation in order

to enhance the ethylene productivity on these systems, e.g. by employing supported $VO(PO_3)_2$ structures with increased surface area while keeping the structural and physico-chemical features of either the bulk or the surface. Modification of the preparation procedures and activation conditions of $(VO)_2P_2O_7$ could also be studied to increase the selectivity to the olefin.

An interesting finding of the present study is the enrichment of vanadium observed on the outermost atomic layer of all the VPO catalysts at 400 ^oC, which contrasts with the frequently reported enrichment of phosphorus in the near surface as observed by XPS.

Acknowledgments

The authors would like to acknowledge the project UV-INV-AE16-484416, and the Fulbright/ME grant FMECD-2011/6543325555, for funding.

References

1. J. G. Speight, Natural gas, the clean fuel: Emissions control and environmental aspects, Hydrocarbon Processing, Jan. (2009).

2. T. Ren, M.K. Patel and K. Blok, Energy 33 (2008) 817-827.

3. J.J.H.B. Sattler, J. Ruiz-Martinez, E. Santillan-Jimenez, B.M. Weckhuysen, Chem. Rev. 114 (2014) 10613-10653.

4. F. Cavani, N. Ballarini, A. Cericola, Catal. Today 127 (2007) 113-131.

5. H.X. Dai and C.T. Au, Current Top. Catal. 3 (2002) 33-80.

6. M.M. Bhasin, Top. Catal. 23 (2003) 1–4.

7. T. Blasco, J.M. López Nieto, Appl. Catal. A: Gen, 157 (1997) 117-142.

8. J.M. López Nieto, P. Botella, M.I. Vázquez, A. Dejoz, Chem. Commun.

17 (2002) 1906-1907.

9. T.T. Nguyen, M. Aouine, J.M.M. Millet, Catal. Commun. 21 (2012) 22-26.

10. B. Solsona, M.I. Vázquez, F. Ivars, A. Dejoz, P. Concepción, J.M. López Nieto, J.Catal. 252 (2007) 271–280.

11. B. Chu, L. Truter, T.A. Nijhuisb, Y. Cheng, Catal. Sci. Technol. 5 (2015) 2807-2813.

12. H. Zhu, P. Laveille, D.C. Rosenfeld, M.N. Hedhilic, J-M. Basset, Catal. Sci. Technol. 5 (2015) 4164-4173.

13. E. Heracleous, A.A. Lemonidou, J. Catal. 237 (2006) 162-174.

14. E. Heracleous, A.A. Lemonidou, J. Catal. 270 (2010) 67-75.

15. B. Solsona, P. Concepción, B. Demicol, S. Hernández, J.J. Delgado, J.J. Calvino, J.M. López Nieto, J Catal. 295 (2012) 104-114.

16. J.M. López Nieto, B. Solsona, R.K. Grasselli, P. Concepción, Top. Catal. 57 (2014) 1248-1255.

17. B. Savova, S. Loridant, D. Filkova, J.M.M. Millet, Appl. Catal. A: Gen. 390 (2010) 148–157.

18. Z. Skoufa, E. Heracleous, A.A. Lemonidou, J. Catal. 322 (2015) 118-129.

19. H. Zhu, D.C. Rosenfeld, D.H. Anjum, V. Caps, J-M Basset, ChemSusChem. 8 (2015) 1254-1263.

20. J.L. Callahan, R.K. Grasselli, AIChE Journal, 9 (1963) 755.

21. N. Ballarini, F. Cavani, C. Cortelli, S. Ligi, F. Pierelli, F. Trifiro, C. Fumagalli, G. Mazzoni, T. Monti, Top. Catal. 38 (2006) 147-156.

22. J.C. Vedrine, G.J. Hutchings, C.J. Kiely, Catal. Today, 217 (2013) 57-65.

23 D.L. Hucknall, “Selective Oxidation of Hydrocarbons” Academic Press 1974.

24 R.L. Varma, D.N. Saraf, Ind. Eng. Chem. Prod. Res. Dev. 18 (1979) 7-13.

25. M.C. Freerks, M. Suda M, US Patent 3832359A (1974), to Monsanto.

26. B. K. Hodnett, Catal. Today 16 (1993) 131-138.

27. G.J. Hutchings, A. Desmartin-Chomel, R. Olier, J.C. Volta, Nature, 368 (1994) 41-45.

28. G.W Coulston, S.R. Bare, H. Kung, K. Birkeland, G.K. Bethke, R. Harlow, N. Herron, P.L. Lee, Science 275 (1997) 191–193.

29. J.K. Bartley, N.F. Dummer, G.J. Hutchings, Vanadium Phosphate Catalysts Metal Oxide Catalysis. S. D. Jackson, J.S.J. Hargreaves (Ed.), WILEY-VCH Verlag, Weinheim (2009), Chapter 12.

30. D. Lesser, G. Mestl, T. Turek, Appl. Catal. A: Gen. 510 (2016) 1–10.

31. V.V. Guliants, J.B. Benziger, S. Sundaresan, I.E. Wachs, J.M. Jehng, J.E. Roberts, Catal. Today 28 (1996) 275-295.

32. F. Cavani, C. Fumagalli, F. Ghelfi, C. Mazzoni, F. Pierelli, EP Patent 1514598 A1 (2005), assigned to Lonza.

33. M.T. Sananes, G.J. Hutchings, J.C. Volta, J. Catal. 154 (1995) 253-260.

34. M. Loukah, G. Coudurier, J.C. Vedrine, M. Ziyad, Microporous Mater. 4 (1995) 345.

35. V.A. Zazhigalov, J. Haber, J. Stoch, L.V. Bogutskaya, I.V.Bacherikova, Appl. Catal. A: Gen. 135 (1996) 155-161.

36. J. Haber, V.A. Zazhigalov, J. Stoch, L.V. Bogutskaya, I.V. Bacherikova, Catal. Today 33 (1997) 39-47.

37. B. Solsona, V.A.Zazhigalov, J.M. López Nieto, I.V. Bacherikova, E.A. Diyuk, Appl. Catal., A: Gen., 246 (2003) 81-92.

38. J.M. López Nieto, V.A.Zazhigalov, I.V.Bacherikova, B.Solsona. Studies in Surface Science and Catalysis, 130B (2000) 1853-1859.

39. M. Gąsior, I. Gressel, V.A. Zazhigalov, B. Grzybowska, Polish Journal of Chemistry 77 (2003) 909-915.

40. V.A. Zazhigalov, E. A. Diyuk, V. V. Sidorchuk, T. I. Mironyuk, Kinetics and Catalysis, 50 (2009) 587–596.

41. L. Lisi, P. Patrono, G. Ruoppolo, J. Mol. Catal. A-Chem. 204-205 (2003) 609-616.

42. P. Ciambelli, L. Lisi, P. Patrono, G. Ruoppolo, G. Russo, Catal. Lett. 82 (2002) 243-247.

43. V.A. Zazhigalov, E. A. Diyuk, V. V. Sidorchuk, Kinetics and Catalysis 55 (2014) 380-389.

44. M. C. Biesinger, L.W.M. Lau, A.R. Gerson, R. St.C. Smart, Appl. Surf. Sci., 257 (2010) 887-898.

45. E. Keimenov, H. Bluhm, M. Hävecker, A. Knop-Gericke, A. Pestryakov, D. Teschner, J.A. Lopez-Sanchez, J.K. Bartley, G.J. Hutchings, R. Schlögl, Surf. Sci., 575 (2005) 181-188.

46. G. W. Coulston, E. A. Thompson, N. Herron, J. Catal., 163 (1996) 122-129.

47. J. Mendialdua, R. Casanova, J. Electron Spectrosc., 71 (1995) 249-261.

48. P. R. Makgwane, E.E. Ferg, D.G. Billing, B. Zeelie, Catal. Lett., 135 (2010) 105-113.

49. N.P. Rajan, G.S. Rao, B. Putrakumar and K.V.R. Chary, RSC Adv., 4 (2014) 53419-53428.

50. F. Cavani, D. D. Santi, S. Luciani, A. Lofberg, E. Bordes-Richard, C. Cortelli and R. Leanza, Appl. Catal., A, 376 (2010) 66-75.

51. G. Busca, G. Martra, A. Zecchina, Catal. Today, 56 (2000) 361-370.

52. B. Solsona, T. Blasco, J. M. López Nieto, M. L. Peña, F. Rey, A. Vidal-Moya, J. Catal. 203 (2001) 443-452.

53. K. Chen, E. Iglesia, A.T. Bell, J. Catal. 192 (2000) 197-203.

54. J. Frey, C. Lieder, T. Schölkopf, T. Schleid, U. Nieken, E. Klemm, M. Hunger, J. Catal. 272 (2010) 131-139.

55. V.V. Guliants, .J.B. Benziger, S. Sundaresan, I.E. Wachs, J.-M. Jehng, J.E. Roberts, Catalysis Today 28 (1996) 275-295.

56. F.B. Abdelouahab, R. Olier, N. Guilhaume, F. Lefebvre, J.C. Volta, J. Catal., 134 (1992) 151-167.

57. R.M. Feng, X.J. Yang, W.J. Ji, Y. Chen, C.T. Au J. Catal., 246 (2007) 166-176.

58. M.L. Granados, F.C. Galisteo, P.S. Lambrou, R. Mariscal, J. Sanz, I. Sobrados, J.L.G.Fierro, A.M. Efstathiou, J. Catal., 239 (2006) 410-421.

59. a) D. Lesser, G. Mestl, T. Turek, Appl. Catal. A: Gen. 510 (2016) 1-10.; b) G. Mestl, D. Lesser, T. Turek, Top. Catal. 59 (2016) 1533-1544.

60. M.T. Sananes, G.J. Hutchings, J.C. Volta, J. Catal., 154 (1995) 253-260.

61. M. Abon, K.E. Bere, A. Tuel, P. Delichere, J. Catal., 156 (1995) 28-36.

62. J.R. Ebner, M.R. Thompson, Catal. Today, 16 (1993) 51-60.

63. M. Ruitenbeek (1999) Characterisation of Vanadium-Based Oxidation Catalysts. Ph.D. Thesis. Utretcht University.

64. H. Morishige, J. Tamaki, N. Miura, N. Yamazoe, Chem. Lett. (1990) 1513-1516.

65. L.M. Cornaglia, C. Caspani, E.A. Lombardo, Appl. Catal., 74 (1991) 15-27.

66. P. Delichère, K.E. Béré, M. Abon, Appl. Catal. A-Gen., 172 (1998) 295-309.

67. L.M. Cornaglia, E.A. Lombardo, Appl. Catal. A-Gen., 127 (1995) 125-138.

68. a) R. Mallada, S. Sajip, C.J. Kiely, M. Menéndez, J. Santamarıa, J. Catal. 196 (2000) 1-7; b) S. Mota, M. Abon, J.C. Volta, J. A. Dalmon, J. Catal. 193 (2000) 308-318.

69. W.P.A. Jansen, M. Ruitenbeek, A.W. Denier v.d. Gon, J.W. Geus, H.H. Brongersma, J. Catal., 196 (2000) 379-387.

70. F. Richter, H. Papp, G.U. Wolf, Th. Götze, B. Kubias, Fresenius J. Anal. Chem., 365 (1999) 150-153.

71. K. Aït-Lachgar-Ben Abdelouahad, M. Roullet, M. Brun, A. Burrows, C.J. Kiely, J.C. Volta, M. Abon, Appl. Catal. A-Gen., 210 (2001) 121-136.

72. B. Horvath, J. Strutz, J. Geyer-Lippmann, E.G. Horvath, Z. Anorg. Allg. Chem., 483 (1981) 181-192.

73. Silversmit, G, Depla, H. Poelman, G.B. Marin, R. De Gryse, J. Electron Spectrosc., 135, (2004), 167-175.

74. L.M. Cornaglia, E.A. Lombardo, J. Phys.: Condens. Matter, 5 (1993) A225.

75. P. Mezentzeff, Y. Lifshitz, J.W. Rabalais., Nucl. Instrum. Methods, B 44 (1990) 296-301.

76. H.H. Brongersma, M. Draxler, M. de Ridder, P. Bauer, Surf. Sci. Rep., 62 (2007) 63-109.

77. F. Richter, H. Papp, Th. Götze, G.U. Wolf, B. Kubias, Surf. Interface Anal., 26 (1998) 736-741.

78. Y. Kamiya, E. Nishikawa, T. Okuhara, T. Hattori, Appl. Catal. A: Gen. 206 (2001) 103-112.

79. B.K. Hodnett, Catal. Rev. Sci. Eng. 27 (1985) 373-424.

80. E.A. Lombardo, C.A. Sanchez, L.M. Cornaglia, Catal. Today, 15 (1992) 407-418.

81. S. K. Wilkinson, M.J.H. Simmons, E.H. Stitt, X. Baucherel, M.J. Watson, J. Catal, 299 (2013) 249-260.

82. E.M. Thorsteinson, T.P. Wilson, F.G. Young, P. H. Kasai, J. Catal., 52 (1978) 116-132.

83. P. Botella, E. Garcıa-Gonzalez, A. Dejoz, J.M. Lopez Nieto, M.I. Vazquez, J. Gonzalez-Calbet, J. Catal., 225 (2004) 428-438.

84. E. Heracleous, A.F. Lee, K. Wilson, A.A. Lemonidou, J. Catal., 231 (2005) 159-171.

85. H. Zhu, H. Dong, P. Laveille, Y. Saih, V. Caps, J.-M. Basset, Catal. Today 228 (2014) 58–64.

86. R. Sanchis, D. Delgado, S. Agouram, M.D. Soriano, M.I. Vázquez, E. Rodríguez-Castellón, B. Solsona, J.M.López Nieto. Appl. Catal. A: Gen. 536 (2017) 18–26.

Table 1. Characteristics of the V-P-O catalysts synthesized.

Catalyst	Precursor	Activation	XRD phases	S_{BET} (m^2g^{-1})
VP1	$VOHPO_4 \cdot 0.5H_2O$	2% ethane in air	$(VO)_2P_2O_7$	9.2
VP1H	$VOHPO_4 \cdot 0.5H_2O$	Helium	$(VO)_2P_2O_7$	15.6
VP2	$VOHPO_4 \cdot 0.5H_2O$	Air	$VOPO_4 \cdot 2H_2O$	2.8
VP3	$VOPO_4 \cdot 2H_2O$	2% ethane in air	$VOPO_4 \cdot 2H_2O$	0.4
VP4	$VO(H_2PO_4)_2$	2% ethane in air	$VO(PO_3)_2$	1.5
VP4H	$VO(H_2PO_4)_2$	Helium	$VO(PO_3)_2$	1.9

Table 2. Oxidative dehydrogenation of ethane on V-P-O catalysts

Catalyst	W/F	Ethane (%)	Selectivity (%)[a]			Productivty		Selectivity[d] at	
	g_{cat} h/ molC_2	Conversion[a]	C_2H_4	CO	CO_2	per mass[a,b]	per surface area[a,c]	2% conv	10% conv.
VP1	8.2	11.2	72.1	2.1	25.8	276	30.0	>98	73.0
VP1H	8.2	14.0	62.3	4.5	33.2	298	19.1	>98	69.0
VP2	41	10.4	32.5	2.0	65.5	23.8	8.5	75.5	35
VP3	164	1.8	77.2	0	22.8	2.37	5.9	77.5	n.a.
VP4	103	9.6	89.9	7.6	2.5	23.4	23.4	>98	89.5
VP4H	103	9.2	89.2	7.9	2.9	22.3	11.7	>98	88.0

[a] Data obtained at 500ºC, C_2/O_2/He = 10/5/85 (molar ratio) for conversions around 10%; [b] Formation rate of product, in $g_{ethylene}/kg_{cat}.h$; [c] Ethylene productivity per surface area, in 10^{-3} $g_{ethylene}$ $m^{-2}{}_{cat}$ h^{-1}; [d] Selectivity to ethylene at 500ºC for ethane conversions of 2 or 10% obtained modifying the contact time to give the desired conversion but maintaining the reaction temperature and the C_2/O_2/He ratio.

Table 3. XPS surface composition of activated V-P-O catalysts measured at 400 ºC

Catalyst	V/O	P/O	P/V	C (%)	O (%)
VP1H	0.12	0.24	2.0	25.4	54.8
VP2	0.15	0.25	1.7	21.4	56.3
VP3	0.15	0.19	1.3	11.5	66.3
VP4H	0.07	0.28	4.2	19.8	57.0

Table 4. V2$p_{3/2}$ XPS binding energies for V-P-O catalysts measured at 400 ºC.

Catalyst	V (V)		V (IV)		V (III)		V^a	V^b	P (V)
	BE (fwhm)	%	BE (fwhm)	%	BE (fwhm)	%	ox. state	ox. state	BE
VP1H	516.7 (2.0)	23	515.6 (2.0)	43	514.3 (2.0)	34	3.9	4.0	132.4
VP2	516.7 (1.5)	17	515.7 (1.9)	72	514.4 (1.6)	11	4.1	4.1	132.6
VP3	516.8 (1.8)	21	515.6 (2.3)	79	-	-	4.2	4.1	132.2
VP4H	-	-	515.6 (2.1)	84	514.5 (1.8)	16	3.8	3.9	132.8

[a)] Average vanadium oxidation state calculated from vanadium species determined by the XPS curve-fitting analysis;

[b)] Average vanadium oxidation state calculated from the splitting between the O(1s) and V($2p_{3/2}$) binding energies by the Coulston equation.

Table 5. Signal intensity ratios for LEISS (using 1000 eV He^+) of V-P-O catalysts measured at 400 ºC.

Catalyst	V/O	P/O	P/V [a)]
VP1H	13.4	0.00	< 0.001 (0.004)
VP2	0.90	0.30	0.33 (1.22)
VP3	0.80	0.15	0.19 (0.70)
VP4H	0.34	0.29	0.85 (3.14)

[a)] In brackets, calculated atomic ratios using relative sensibility factor from ref. [66].

Table 6. Representative results reported in the literature for the oxidative dehydrogenation of ethane.

Catalyst	C_2/O_2/inert molar ratio	T /ºC	Selectivity[a] 10% conversion	W/F [b] /g s cm^{-3}	C_2 conv.[c] /%	$Y_{C2=}$[d] /%	Areal rate[e]
MoVNb	9/6/85	350	64	-	58	38	-
MoVTeNb	30/30/40	400	96	3.2	84	80	$4.1.10^{-4}$
NiNbO	9.1/9.1/81.8	400	92	0.54	66	46	$0.53.10^{-4}$
$NiNbO/Al_2O_3$	9.1/9.1/81.8	400	90	0.6	27	19	$0.16.10^{-4}$
NiWO	10/10/80	400	68	0.6	52	31	$0.38.10^{-4}$
Ni/TiO_2	10/10/80	450	90	0.23	41	30	$2.0.10^{-4}$
VPO[f]	10/5/85	500	73	0.12	22	15	$8.1.10^{-4}$
VPO[g]	10/5/85	500	89	1.51	10	9	$1.8.10^{-4}$

[a] selectivity to ethylene at 10% conversion at the temperature indicated (different contact times)
[b] pseudo-contact times (W/F) equivalent to the weight of catalyst (g) divided by the feed gas flow rate at operating conditions ($cm^3\ s^{-1}$)
[c] conversion of ethane at the temperature and W/F shown
[d] per pass yield of ethylene at the temperature and W/F shown
[e] areal rate in mmol ethane reacted per m^2 and per s (mmol $m^{-2}\ s^{-1}$)
[f] corresponds to VP1 from the present article
[g] corresponds to VP4 from the present article

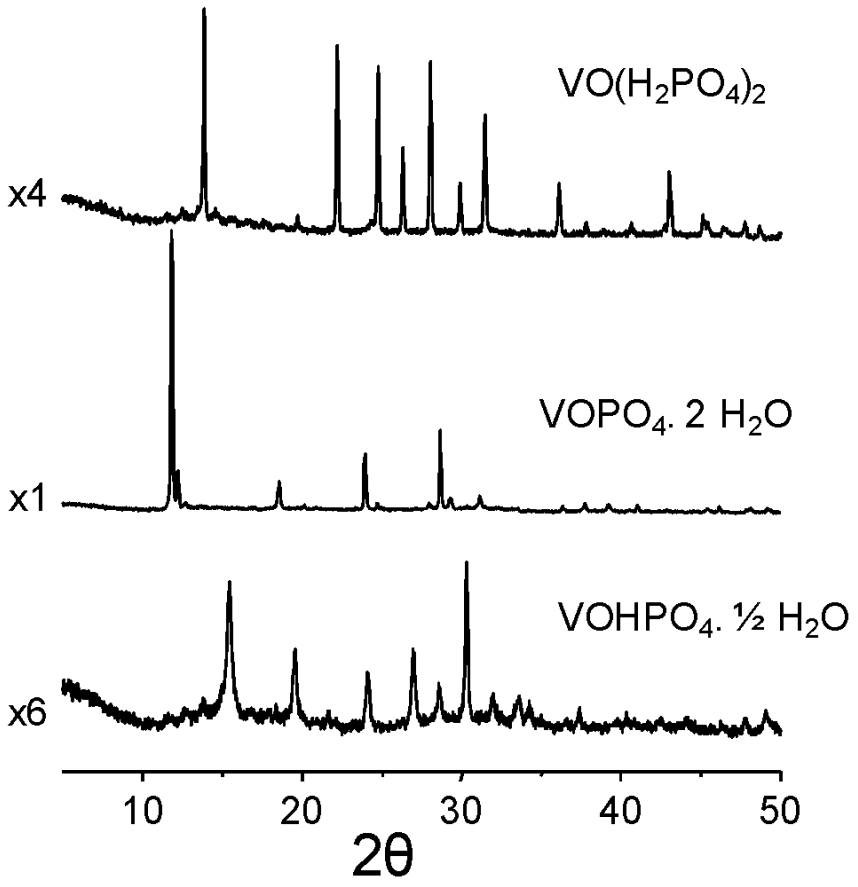

Figure 1. XRD patterns of V-P-O precursors.

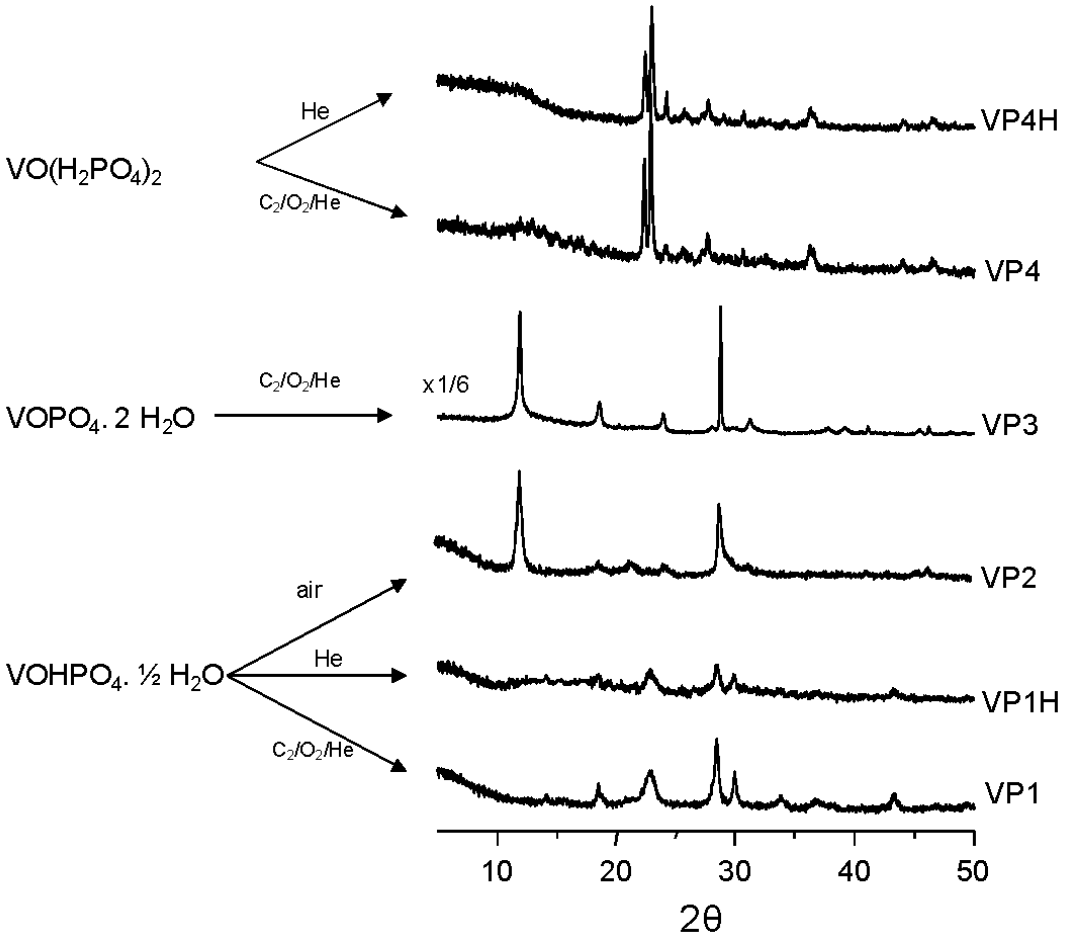

Figure 2. XRD patterns of activated V-P-O catalysts.

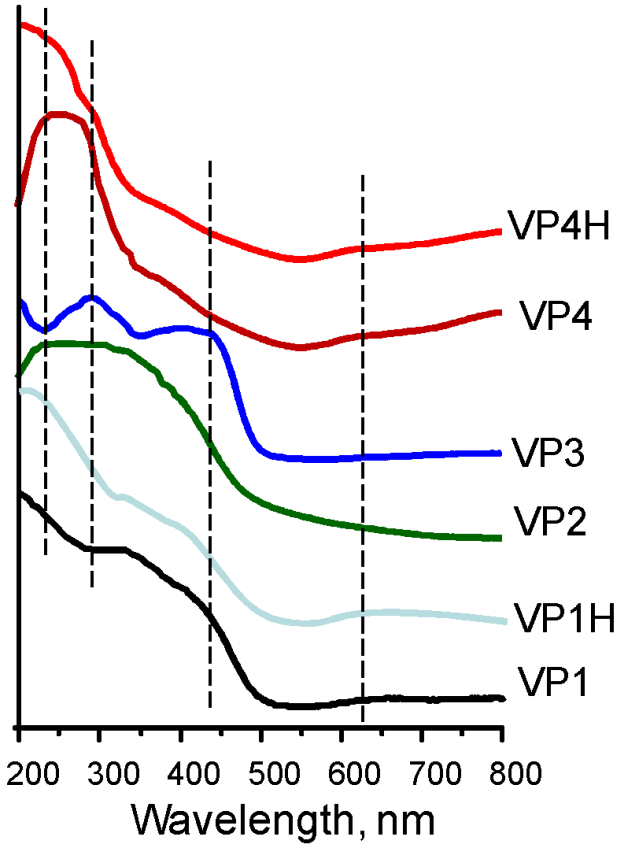

Figure 3. DR-UV-Vis. spectra of activated V-P-O catalysts.

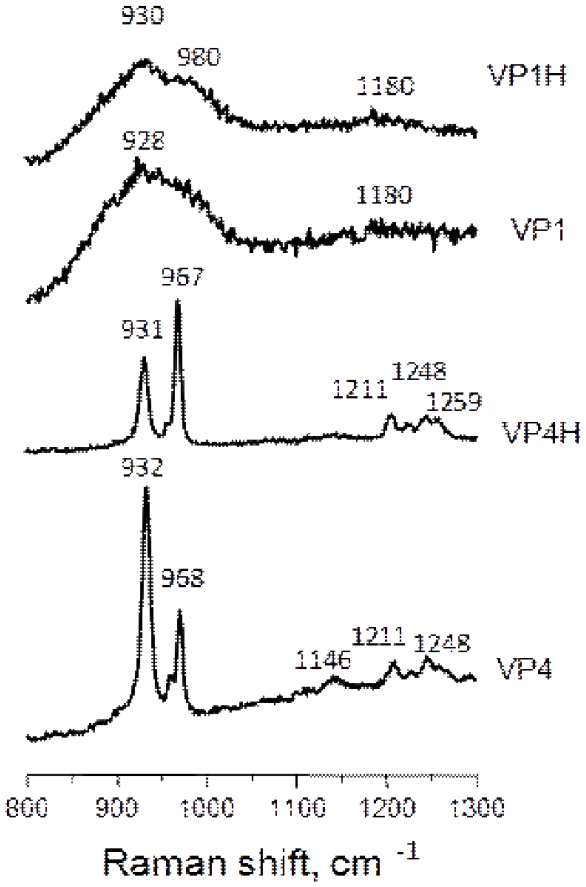

Figure 4. Raman spectra of activated V-P-O catalysts

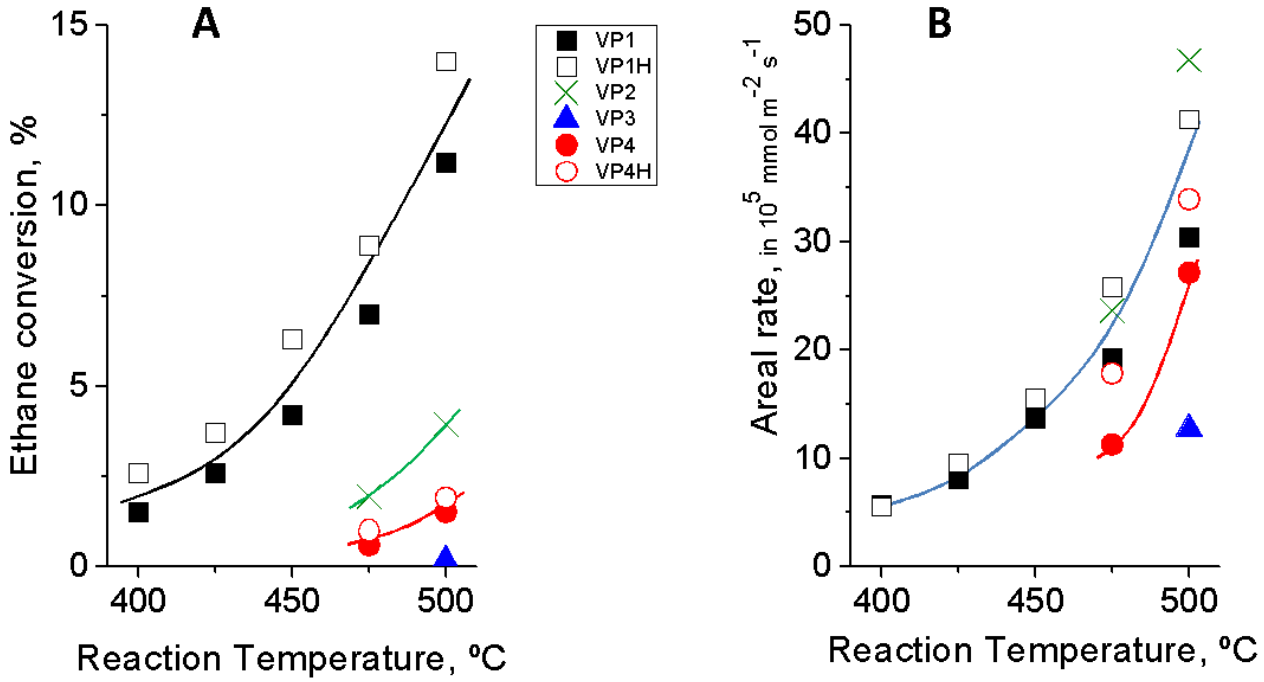

Figure 5. Evolution of the ethane conversion (A) and the areal rate (B) with the reaction temperature. Reaction conditions as detailed in the text, with a fixed contact time of 8 g_{cat} h/ molC_2. C_2H_6/O_2/He: 10/5/85 molar ratio.

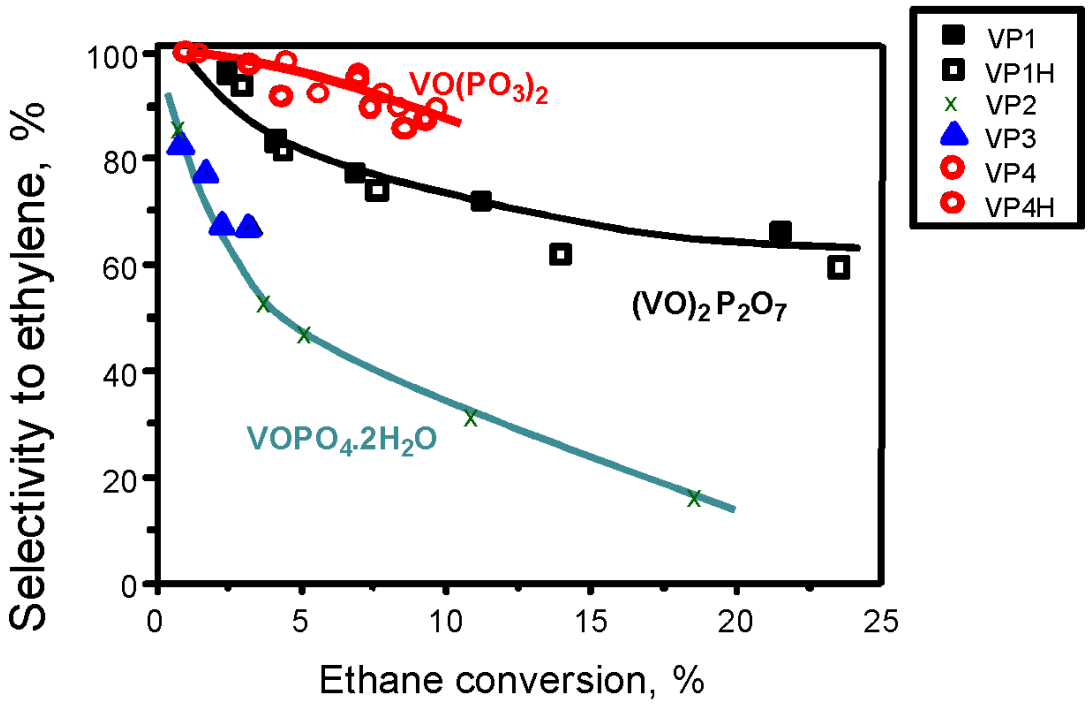

Figure 6. Variation of the selectivity to ethylene with the ethane conversion at a reaction temperature of 500ºC. **Note:** The C_2H_6/O_2/He: 10/5/85 molar ratio has been maintained constant, but the contact time has been modified by changing either the catalyst weight and/or the total flow with the aim of obtaining different ethane conversions. Remaining reaction conditions as detailed in the text.

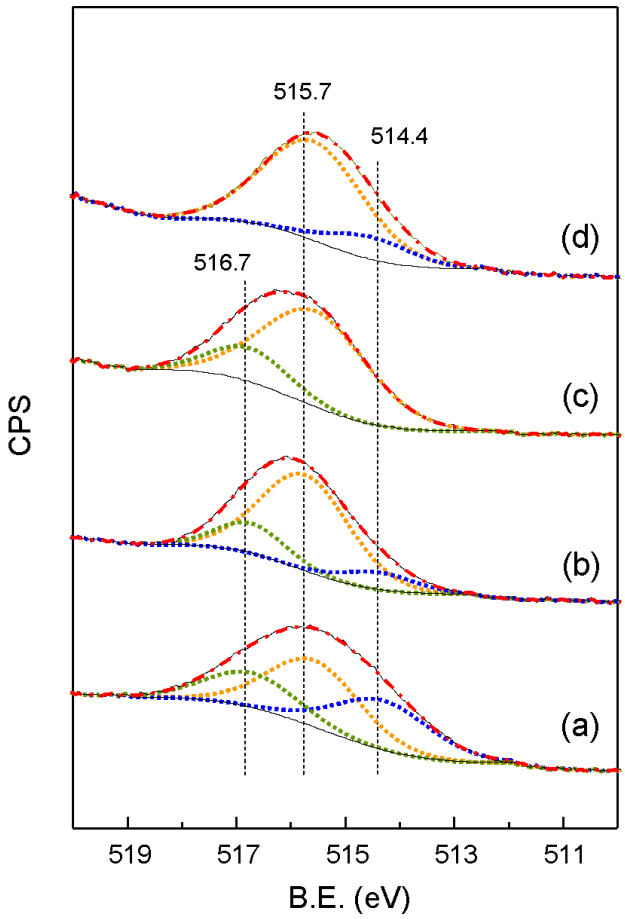

Figure 7. Curve fitting analysis of XPS V($2p_{3/2}$) core level for V-P-O catalysts at 400 ºC: a) VP1H, b) VP2, c) VP3, d) VP4H. Components calculated at 516.7 (green), 515.7 (orange) and 514.4 (blue); resultant envelop (red); original spectra (black).

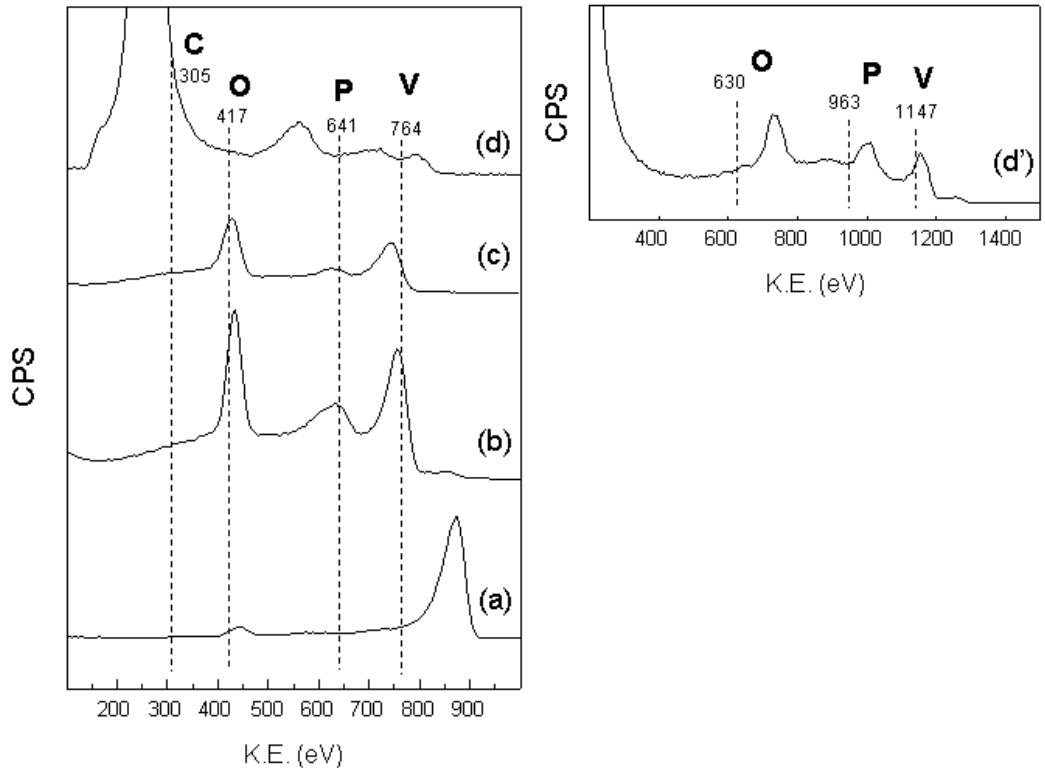

Figure 8. LEIS spectra collected for 1000 eV He^+ beam scattered from V-P-O catalysts at 400 ºC: a) VP1H, b) VP2, c) VP3, d) VP4H. Higher resolution LEIS spectra collected on VP4H using 1500 eV He^+ is also included (d') to confirm the peak assignment. Dashed lines indicate the theoretical scattering energies for single elastic collision of He^+ with the corresponding element at the experimental conditions described in the text.

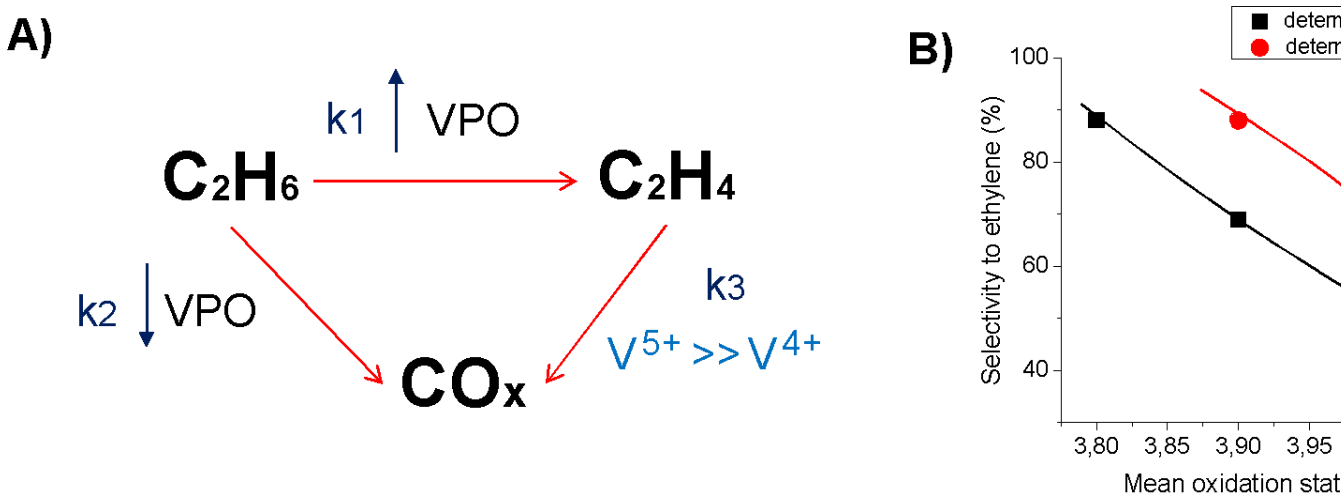

Figure 9. A) Reaction scheme of V-P-O catalysts in the oxidation of ethane; B) Relationship between the selectivity to ethylene (at 500ºC and 10% ethane conversion) with the mean oxidation state of vanadium determined from XPS data by curve fitting analysis (■) or by Coulston equation (●).